ANL-HEP-CP-85-18
For the Proceedings of the
San Miniato Topical Seminar
San Miniato, Italy March 1985
ConF-8503146--1

SUMMARY OF S = 0 DIBARYON RESONANCES AND CANDIDATES

Akihiko Yokosawa

High Energy Physics Division
Argonne National Laboratory, Argonne, Illinois USA

18 April 1985

ANL-HEP-CP--85-18

DE85 012125

Abstract

We review experimental data concerning S = 0 dibaryon resonances, with an emphasis on the nucleon-nucleon system. Structures observed in the γd channel, the πd elastic scattering, pp → πd channel, and other channels are discussed. Experimental data are compared with various theories. The short-range forces can be represented by dibaryon resonances. Further measurements to clarify the understanding of dibaryons are also discussed.

For nearly one decade, an extensive search for dibaryon resonances in the various reactions in the NN, πd, γd, and other channels has been made. Many structures were found in the NN system and they were investigated by means of phase-shift analyses. The results confirmed Breit-Wigner behavior for some of them and these resonances are now well established. Structures observed in the NN, πd and γd channels are not explained by the standard theories, with the exception of some phenomenological models, and are well explained by adding the dibaryon admixture to theoretical models.

As evidence for the existence of dibaryons grows, it becomes crucial to understand the nature of these resonances. Earlier references to theoretical work (MIT bag model, string model, spring model, πNN and $\pi\pi$NN dynamics, Deck model, OPE three-body theory, OBE inelastic-threshold model, coupled-channels method etc.) were discussed in Ref. 1. Recent references are discussed in this paper. One nice way to clarify the nature of resonances is to thoroughly study the isospin-zero channels in the region where there is no Δ excitation. Structures were seen in the existing $\Delta\sigma_L(I = 0)$ data, although these are yet to be confirmed. We are expecting various experimental data in this channel in a few years.

We start with discussing structures in the NN channel and compare these with structures in other channels (πd, γd, etc.).

I. Nucleon-Nucleon System

A detailed description on the notation and definition of the spin observables is given in Ref. 1.

A. I = 1 System

A striking energy dependence has been observed in the difference between the proton-proton total cross sections for pure spin states:

$$\Delta\sigma_L = (4\pi/k)\ \mathrm{Im}\{\phi_1(0) - \phi_3(0)\} = \sigma^{\mathrm{Tot}}(\tfrac{+}{+}) - \sigma^{\mathrm{Tot}}(\tfrac{+}{-})$$

and

$$\Delta\sigma_T = -(4\pi/k)\ \mathrm{Im}\ \phi_2(0) = \sigma^{\mathrm{Tot}}(++) - \sigma^{\mathrm{Tot}}(+-)\ .$$

In the $\Delta\sigma_L$ energy dependence, structures responsible to R_J (singlet) and $R_{J\pm1,J}$ (coupled triplet) appear as peaks and dips respectively. On the other hand, in the $\Delta\sigma_T$ energy dependence, R_J and R_{JJ} (uncoupled triplet) emerges as peaks and dips respectively.

The beginning of the excitement observing structures in the pp system was from $\Delta\sigma_L$ measurements as shown in Fig. 1[2] followed by Fig. 2.[3] Figures 3 and 4 show $\Delta\sigma_T$ data.[4,5] All the data in Fig. 1 were obtained at the Argonne ZGS. In Fig. 2 one observes systematic differences between the BASQUE data and the rest of the data taken at LAMPF, Argonne ZGS, SIN, and SATURN II (note that SATURN II data are not shown in Fig. 2). In Fig. 4 selected data from Ref. 5 are shown. We observe a narrow peak with ~ 40-MeV width at p_{lab} = 1.15 GeV/c (mass, 2.14 GeV). Large energy dependence is also seen in the polarization parameters, C_{NN} = (N,N;0,0), and C_{LL} = (L,L;0,0), as reported in Ref. 1.

Various analyses have been carried out using presently available data to clarify the nature of the structure in the proton-proton system. Particularly strong indication of resonances in the $^1D_2$ ($B_1{}^2$ (2.14)) and $^3F_3$ ($B_1{}^2$(2.22)) states are established in the phase-shift analyses.[6-8] An attempt was made to test some of the pre-existing phase-shift solutions by comparing the experimental values[9] of C_{LL} = (L,L;0,0) and C_{SL} = (S,L;0,0) at 1.18 to 2.47 GeV/c and of C_{SS} = (S,S;0,0) at 487 to 791 MeV with their predictions. The results are shown in Fig. 5. By using the C_{LL} data and the dispersion relations, values of $\Delta\sigma_L$ (inelastic) were calculated.[9a] The results are shown in Fig. 6 and compared with theoretical predictions[10] which do not include diproton resonances. Existing theoretical models such as π-exchange or OBE models (not phenomenological models) developed in describing medium- and long-range forces, but not short-range force, breakdown rapidly with increasing energy.

The $^1D_2$ and $^3F_3$ partial waves in the Argand diagram are shown in Figs. 7 and 8. The polarization transfer parameters K_{SS}, K_{LS}, K_{SL}, and K_{LL} at 597 to 800 MeV were measured.[11] The data are in satisfactory agreement with

pre-existing phase-shift analyses. Resonances poles with $J^P = 2^+$, 2^-, and 3^- found by K-matrix analysis are discussed by several authors.[12] The $\Delta\sigma_L$(inelastic) data discussed above are explained by the Deck model with the dibaryon admixture[13] or by dibaryon resonances ($^1D_2$ plus $^3F_3$) alone.[6] It is conceivable that the short-range force is represented by dibaryon resonances. One could conclude that the existence of baryon-baryon resonances is in exotic quark configurations.

We review other structure in the pp system besides the $^1D_2$ and $^3F_3$ states. Other possible resonances include a singlet resonance in $\Delta\sigma_T$ (see Fig. 3) at 2 GeV/c, $^1G_4$ ($B_1{}^2(2.43)$), and a triplet resonance appearing in $(k^2/4\pi)$ $(\Delta\sigma_T - \Delta\sigma_L)$ plot as shown in Fig. 9. We expect that the triplet peak at 2.0 GeV/c is due to a resonating partial wave R_{JJ} ($B_1{}^2(2.43)$), since only R_{JJ} term has positive sign in

$$\Delta\sigma_T - \Delta\sigma_L \propto (2J + 1)\mathrm{Im}R_{JJ} - (J + 2)\mathrm{Im}R_{J+1,J} - (J - 1)\mathrm{Im}R_{J-1,J} .$$

We note that there is no $^3F_3$ partial-wave contribution to the polarization data at $\theta_{c.m.} = 63°$. We see an interesting structure in plot of $k^2P(d\sigma/d\Omega)/\sin\theta_{c.m.}$ with respect to p_{lab} as shown in Fig. 10. The quantity is proportional to

$$(2\mathrm{Im}^3P_0 + 3\ \mathrm{Im}^3P_1)(\mathrm{Re}^3P_2) - (2\mathrm{Re}^3P_0 + 3\mathrm{Re}^3P_1)\ (\mathrm{Im}^3P_2)$$

if higher partial waves are neglected.

This energy region has been investigated by measuring C_{LL} around $\theta_{c.m.} = 90°$. Figure 11 shows a plot of $k^2(C_{NN} - C_{LL})\ d\sigma/d\Omega$ at $\theta_{c.m.} = 90°$.[14] This quantity contains only coupled spin-triplet partial waves with $J = L \pm 1$

(such as $^3P_0$, $^3P_2$, $^3F_2$, $^3F_4$...). The dashed curve shows a rapid energy dependence in $(1 - C_{NN})$, and the peak position roughly coincides with the $^1D_2$ resonance. This leads us to note that the structure in the $(C_{NN} - C_{LL})$ curve is therefore also resonant-like. The $^3P_0$ or $^3P_2$ state, $B_1{}^2$ (2.18), are probably responsible for the structure. We note that a model of coupled nucleon and isobar channels predicts a resonant structure in the $^3P_0$ channel as well as in the $^1D_2$ and $^3F_3$ resonant structures.[15]

Do we observe any structure above a mass of 2500 MeV? A possible structure beyond this energy region has been searched for by measuring the parameter C_{LL} around $\theta_{c.m.} \approx 90°$.[16] Figure 12 shows the energy dependence of $k^2 C_{LL}\ d\sigma/d\Omega$. We now attempt to interpret these structures by assuming them to be resonances in terms of the quantum numbers. We note that

$$k^2\ C_{LL}\ d\sigma/d\Omega \approx -|\text{spin-singlet terms}|^2 - |\text{coupled triplet}|^2 + |\text{uncoupled and coupled triplet}|^2 .$$

We observe no structure in the behavior of $k^2\ (C_{NN} - C_{LL})\ d\sigma/d\Omega$, which contains only coupled triplet terms. Therefore, the second dip seems to be due to a spin-singlet term; in a similar way, the first dip is attributed to a spin-singlet term, namely, $^1G_4$. It is possible to attribute the second dip (mass $\approx 2900 \pm 100$ MeV) to a $^1I_6$ state because the dip around $\theta_{c.m.} \approx 90°$ disappears at $\theta_{c.m.} \approx 75°$, where $P_6(\cos\theta) = 0$.[16] The bump may be considered as a R_{JJ} ($B_1{}^2$ (2.70)).

B. I = 0 System

Measurements of the difference between isoscalar nucleon-nucleon total cross sections for pure longitudinal initial spin states, $\Delta\sigma_L(pd)$, were performed using a polarized proton beam and a polarized deuteron target.[17]

One can extract $\Delta\sigma_L(I = 0)$ data using both $\Delta\sigma_L(pd)$ and $\Delta\sigma_L(pp)$ as shown in Fig. 13. A significant structure is observed around 1.5 GeV/c. From the dispersion analysis of a forward I = 0 scattering amplitude using the data on $\Delta\sigma_L(I = 0)$, Grein and Kroll[18] showed that the Argand plot of the amplitude has a resonance-like behavior around 1.5 GeV/c.

The polarization parameters of the pn elastic scattering were measured at KEK covering beam momenta from 1.30 to 1.82 GeV/c.[19] The data are consistent with earlier predictions of the resonant-like behavior in singlet state $^1F_3$ (2190).[20] Measurements of many other parameters are obviously needed for the I = 0 phase-shift analyses.

An extensive study[21] on the I = 0 system is being undertaken at LAMPF (Los Alamos) using polarized neutron beams.[22] A longitudinally polarized neutron beam is produced at forward angles when a longitudinally polarized proton beam strikes a deuteron target. In the energy interval of 500 to 800 MeV polarization value is ~ 50%. The measurements include n-p elastic-scattering observables C_{SS}, C_{LS}, C_{LL} etc. of a wide angular range at energies of 500, 630, and 800 MeV. Preliminary data show that predictions from presently available np phase-shift solutions are rather good. The total cross section measurements with spin will also be performed. We expect the experimental results will clarify the structure in I = 0 system.

We note that the np total cross-section data show no evidence for narrow resonances in a mass range below 2.23 GeV.[23]

C. $NN \to NN\pi$

For lab momenta between 1 and 2 GeV/c, several sets of $NN \to NN\pi$ data are available. The reaction cross sections for $pp \to pn\pi^+$, $pp\pi^0$ (Ref. 24) and $np \to pp\pi^-$ (Ref. 25) are shown in Fig. 14 where the Deck model predictions with and without dibaryon admixture $^3F_3$ (B_1^2 (2.22)) are also shown.[13]

The inelastic cross sections in longitudinal spin states, $\Delta\sigma_L^{in}$, are discussed in Section A.

D. Conclusions on I = 0 and I = 1 Resonances in the Nucleon-Nucleon System

Candidates for dibaryon resonances that can couple to nucleon-nucleon systems are summarized in Table I.

II. Dibaryon Resonances in γd Scattering Experiment

The measured $\gamma d \to pp\pi^-$ cross section shows a rapid variation around a photon energy k = 390 MeV as shown in Fig. 15.[26] The peak has been interpreted by the existence of a dibaryon resonance at a mass of 2.23 GeV/c^2 with a width of 40 MeV/c^2. This observation is consistent with the existence of $^3F_3$ ($^3_1$ (2.22)) resonant state discussed above.

Earlier a dibaryon resonance (mass of 2380) has been suggested by interpreting the result of $\gamma d \to p^+n$.[27] However, the prediction by a model used to interpret the data has recently been experimentally tested,[28] as shown in Fig. 16, and it seems necessary to repeat the analysis using the new information.

III. Dibaryon Resonances in πd Elastic Scattering

i) Cross-Section Measurements

It has been shown by several authors that there are effects of dinucleon resonances in πd elastic scattering.[29,30] The effects are clearly seen in the angular region of $\theta_{c.m.} > 100°$. We note that the forward region is well described by a Faddeev-type multichannel scattering theory, and the short-range behavior seems to appear at larger angles. Measurements in backward π^-d elastic scattering were carried out at KEK. The data show two bumps at around 670 and 1100 MeV/c, two dips near 630 and 980 MeV/c, and a break at 550 MeV/c (see Fig. 17).[31] The results of a phenomenological fit is consistent with the existence of three dibaryon resonances with mass of 2.362,

2.429, and 2.722 GeV in this energy region.

ii. Tensor Polarization

The tensor polarization t_{20} of π^+d elastic scattering has been measured at T_π = 120 and 138 MeV at SIN as a function of scattering angle.[32] While at the higher energy a strong oscillatory behavior prevails, a considerable flattening is observed at the lower energy as shown in Fig. 18. The results are interpreted by including three dibaryon resonances, $^1D_2$, $^3F_3$, and $^1G_4$. However, a similar experiment[33,34] at LAMPF disagrees with the SIN data, although the measurements were at T_π = 142 MeV. In Fig. 18 only the earlier data are shown but they are in agreement with new data.[33] We need to wait for the clarification.

iii. Vector Polarization

In the measurement of the vector polarization (iT_{11}) in elastic $\pi d^\dagger$ scattering at T_π = 140 to 294 MeV, evidence for a dibaryon signal has been found (see Fig. 19).[35] The striking oscillations observed in the vector polarization are not reproduced by conventional Faddeev amplitudes. The data were interpreted by including at least one of the three proposed B = 2 resonances [$^1D_2$ ($B_1{}^2(2140)$), $^3F_3$ ($B_1{}^2(2220)$), and $^1G_4$ ($B_1{}^2(2430)$)] with the result of Faddeev calculations. At the higher energies the general trend of the data favors the admixing of the $^1G_4$ dibaryon resonance.

At KEK the vector polarization for the π^+d elastic scattering was measured at 0.74 and 1.50 GeV/c.[36] The measurements cover a higher energy region than those investigated so far. The results are being interpreted.

IV. $pp \to d\pi^+$ Reaction

Earlier H. Kamo and W. Watari found the effects of dinucleon resonances in the polarization data in $pp \to \pi d$ reaction.[37]

Many measurements of the cross section and polarization have been made in the energy range 400 to 1300 MeV.[38] The $d\pi^+$ system has also been studied with polarized deuterons in the pp final state.[39] The parameters of A_{NN} and A_{LL} for the $pp \to d\pi^+$ reaction were measured at 1.28 and 1.46 GeV/c for the deuteron angles between 2.25° and 7.75° at LAMPF, and the data are being analyzed.[40]

Partial-wave analyses[41] using the global data in this channel contribute significant information about the existence of highly inelastic dibaryon resonances. Measurements of spin-correlation parameter A_{NN} and polarization parameters[42] at 90° between 500 and 800 MeV are useful to test predictions of the PWA analyses and improve the solutions. The results are included in a recent energy-independent PWA analyses.[43]

Polarization measurements for $p^{\uparrow}p \to d\pi^+$ from T_p = 1.0 to 2.3 GeV have been carried out at Saclay.[44] Preliminary results have a peak at 140° c.m. around $T_p \approx 1.9$ GeV (near 2700 MeV mass) as shown in Fig. 20. This is interpreted as a possible candidate for the q^6, structure near the energy predicted by the Cloudy Bag Model.[45,46] In Table I, $B_1{}^2(2.70)$ with quantum number triplett R_{JJ} is shown.

V. Structures Revealed in the Nucleon-Nucleon Mass Spectrum

The $dp \to (pn)p$ break-up reaction at 3.3-GeV/c deuteron momentum was studied using films from 1-m hydrogen bubble chamber.[47] The effective mass distribution of two nucleons exhibits enhancements at M_{pn} = 2020 MeV with Γ = 45 ± 20 MeV and 2130 MeV with Γ = 20 ± 10 MeV. The $dp \to (p\pi^+)$ + missing mass reaction was also studied.[47] Structures were observed in nn and $nn\pi^+$ invariant mass spectra. The nn system shows mass enhancements at 2.03 and 2.14 GeV. The $nn\pi^+$ mass spectra exhibits enhancement at 2.390 GeV (Γ = 42 ± 20) as shown in Figs. 21-23. These measurements are being remeasured by a

Tokyo group (bubble chamber experiment) and a Kyoto group (counter experiment) at KEK, and the results are expected soon.

VI. Narrow States in Missing-Mass Spectra

The missing-mass spectra for the reaction $p + {}^3He \to d + X$ and ${}^3He + p \to d + X$ have been measured at $T_{{}^3He} = 2.7$ GeV and $T_p = 0.925$ GeV respectively at the Saturne National Laboratory (see Fig. 24).[48,49] There is an indication for a narrow structure at 2.12 GeV. Similar mass and width have been found in the deuteron break-up study.[47] The data also show a narrow structure with a mass $M = 2.240 \pm 0.005$ GeV and a width $\Gamma_{1/2} = 0.016 \pm 0.003$ GeV. It is interesting to note that this mass coincides with $B_1{}^2(2.22)$ in the ${}^3F_3$ state. Further studies in this reaction are underway at Saclay.

VII. Summary

During the past several years, extensive search for structures, which could be related to the existence of dibaryons, has been made in various reactions. The dinucleon resonance opened a new era in the nucleon-nucleon system and is crucially important for the development of the quark models that require six quarks in a bag although many other interpretations without the quark concept exist.

Structures discovered in various reactions are in general not explained by standard theoretical models without the admixing of dibaryon resonances. The results of existing proton-proton phase-shift analyses by various authors are in good agreement; resonant-like behavior is found in ${}^1D_2$ and ${}^3F_3$ states. The nature of these resonances are considered as:

i) Unconventional resonances (caused by short-range forces); existence of six-quark state dibaryon resonances.[50] Measurements as shown in Fig. 6 clearly demonstrate the need of short-range forces which are represented by dibaryon resonances.

ii) Conventional resonances (caused by ordinary medium to long range meson-exchange forces); channel-coupling effects (NN to NΔ, πD)[51] or other nuclear theoretical techniques.[52]

Since the I = 0 channel cannot couple to NΔ or πD channels, discovery of I = 0 resonances below mass 2200 MeV would support the existence of exotic quark states. The study is underway, as described in Section I-B.

In order to determine further whether dibaryon resonances are caused by exotic quark configurations, the following attempts should be made:

a) Spin measurements above the $^3F_3$ resonances to clarify high-mass candidates $B_1{}^2$ (2.42), $B_1{}^2$ (2.70), and $B_1{}^2$ (2.90).

b) Confirmation of the $B_0{}^2$ (2.22) resonance by utilizing polarized neutron beams.

c) Accurate measurements in those channels discussed above which produced narrow-width resonances, $^1D_2$ ($B_1{}^2$ (2.14)) and $^3F_3$ ($B_1{}^2$ (2.22)).

TABLE I

Candidates of the Dinucleon Resonances

(i) I = Isospin State

	$B_1^2(2.14)$	$B_1^2(2.18)$	$B_1^2(2.22)$	$B_1^2(2.43)$	$B_1^2(2.43)$	$B_1^2(2.70)$	$B_1^2(2.90)$
Mass, GeV	2.14 - 2.17	2.18 - 2.20	2.20 - 2.25	2.43 - 2.50	2.43 - 2.50	2.70 ± 0.10	2.90 ± 0.10
Width, MeV	50-100	100-200	100-200	~ 150	~ 150		
Quantum State	$^1D_2$	Triplet P ($^3P_0$ or $^3P_2$)	$^3F_3$	Probably $^1G_4$	Triplet R_{JJ}	Triplet R_{JJ}	Probably $^1I_6$

ii) I = 0 Isospin State

	$B_0^2(2.22)$	$B_0^2(2.43)$
Mass, GeV	2.20 - 2.26	2.40 - 2.50
Width, MeV	100-200	
Quantum State	$^1F_3$	Triplet

Note - Fewer candidates in I = 0 compared to I = 1 are merely due to the lack of experimental data; many experimental attempts will be made to explore the I = 0 state.

REFERENCES

1. A. Yokosawa, Phys. Reports 64, (1980); and references therein.
2. I. P. Auer et al., Phys. Lett. 67B, 113 (1977); I. P. Auer et al., Phys. Lett. 70B, 475 (1977); I. P. Auer et al., Phys. Rev. Lett. 41, 354 (1978).
3. I. P. Auer et al., Phys. Rev. D24, 2008 (RC) (1981); I. P. Auer et al., Phys. Rev. D29, 2435 (1984); J. P. Stanley et al., Nucl. Phys. A403, 525 (1983); J. Bystricky et al., Phys. Lett. 142, 130 (1984); and references therein.
4. W. deBoer et al., Phys. Rev. Lett. 34, 558 (1978); E. K. Biegert et al., Phys. Lett. 73B, 235 (1978); data points at 1.2 and 1.5 GeV/c are being revised (J. B. Roberts, private communication).
5. W. R. Ditzler et al., Phys. Rev. D27, 680 (1983); W. P. Madigan et al., Phys. Rev. D5, 966 (1985).
6. N. Hoshizaki, talk given at 7th Int. Seminar on High Energy Physics, Dubna, June, 1984; earlier references are listed in Ref. 1.
7. R. Bhandari et al., Phys. Rev. Lett. 46, 1111 (1981); R. A. Arndt et al., Phys. Rev. D28, 97 (1983).
8. Saclay-Geneva analysis, J. Bystricky et al., to be published in Phys. Rev.
9. (a) I. P. Auer et al., Phys. Rev. Lett. 51, 1411 (1983).
   (b) W. R. Ditzler et al., Phys. Rev. D29, 2137 (RC) (1984).
10. A. König and P. Kroll, Nucl. Phys. A356, 345 (1981); W. M. Kloet and R. R. Silbar, Nucl. Phys. A364, 346 (1981); A. S. Rinat and R. S. Bhalerao, Weizmann Institute, Report No. WIS-82/55 Nov.-Ph. (1982).

11. C. L. Hollas et al., Phys. Rev. C30, 1251 (1984).

12. Ref. 7; B. J. Edwards and G. H. Thomas, Phys. Rev. D22, 2772 (1980); B. J. Edwards, Phys. Rev. D23, 1978, (1981); T. Ueda, Phys. Lett. 119B, 281 (1982); N. Hiroshige et al., Prog. Theor. Phys. 72, 1287 (1984); N. Hiroshige, M. Kanasaki, W. Watari, and M. Yonezawa, to be published in Prog. Theor. Phys.

13. W. Jauch et al., Phys. Lett. 143B, 509 (1984); WUB 84-7 (1984); and references therein.

14. G. R. Burleson et al., Nucl. Phys. B213, 365 (1983); and references therein. For other C_{NN} data, T. S. Bhatia et al., Phys. Rev. Lett. 49, 1135 (1982).

15. E. L. Lomon, Phys. Rev. D26, 576 (1982); to be published in Phys. Rev. D, Comments Section (1985).

16. I. P. Auer et al., Phys. Rev. Lett. 48, 1150 (1982).

17. I. P. Auer et al., Phys. Rev. Lett. 46, 1177 (1981).

18. W. Grein and P. Kroll, Nucl. Phys. A377, 505 (1982).

19. M. Sakuda et al., Phys. Rev. D25, 2004 (RC) (1982).

20. K. Hashimoto et al., Prog. Theor. Phys. 64, 1678 (1980); 64, 1693 (1980).

21. LAMPF elastic-scattering experiments E-665/770, and E-589/861, followed by E-683, $\Delta\sigma_L$ and $\Delta\sigma_T$ measurements.

22. J. S. Chalmers et al., Phys. Lett. (1985).

23. P. W. Lisowski et al., Phys. Rev. Lett. 49, 255 (1982).

24. F. Shimizu et al., Nucl. Phys. A386, 571 (1982).

25. L. G. Dakhno et al., Phys. Lett. 114B, 409 (1982).

26. P. E. Argan et al., Phys. Rev. Lett. 46, 96 (1981).

27. H. Ikeda et al., Nucl. Phys. B172, 509 (1980); K. Fujii et al., Nucl. Phys. B187, 53 (1981); and references therein.

28. K. H. Althoff et al., 6th Int. Symp. on High Energy Spin Physics, Marseilles, France (1984).

29. K. Kanai et al., Prog. Theor. Phys. 62, 153 (1979); K. Kanai and A. Minaka, Prog. Theor. Phys. 65, 266 (1981).

30. K. Kubodera et al., Phys. Lett. 87B, 169 (1979); J. Phys. G6, L1 (1980); M. P. Locher and M. E. Sainio, Phys. Lett. 121B, 227 (1983).

31. M. Akemoto et al., Phys. Rev. Lett. 50, 400 (1983); 51, 1838 (1983).

32. W. Grüebler et al., Phys. Rev. Lett. 49, 444 (1982).

33. J. Holt et al., Phys. Rev. Lett. 47, 472 (1981).

34. E. Ungricht et al., to be published in Phys. Rev. C (1985).

35. J. Bolger et al., Phys. Rev. Lett. 46, 167 (1981); 48, 1667 (1982); G. Smith et al., Phys. Rev. C29, 2206 (1984).

36. I. Yamauchi et al., to be published (1985).

37. H. Kamo and W. Watari, Prog. Theor. Phys. 62, 843 (1979); H. Kamo et al., Prog. Theor. Phys. 64, 2144 (1980).

38. J. Hoftiezer et al., Nucl. Phys. A412, 273 (1984); A412, 286 (1984); E. Aprile et al., Nucl. Phys. A415, 365 (1984); and references therein.

39. E. Ungricht et al., Phys. Rev. Lett. 52, 333 (1984); and references therein.

40. G. Pauletta et al., to be published.

41. N. Hiroshige et al., Prog. Theor. Phys. 68, 2074 (1982); D. V. Bugg, J. Phys. G: Nucl. Phys. 10, 47 and 717 (1984); and references therein.

42. G. Glass et al., Phys. Rev. Lett. 53, 1984 (1984).

43. For instance, see N. Hiroshige et al, Prog. Theor Phys. 72, 1146 (1984). For comprehensive review, see M. P. Locher, the 6th International Symposium on High Energy Spin Physics, Marseilles, France, September, 1984.

44. R. Bertini et al., Grenoble-Lyon-Saclay collaboration.

45. E. L. Loman, PANIC X Heidelberg, July 1984.

46. P. J. Mulders and A. W. Thomas, J. Phys. G9, 1159 (1983).

47. T. Siemialczuk et al., Phys. Lett. 128B, 367 (1983); to be published in Phys. Lett. (1984).

48. B. Tatischeff et al., Phys. Rev. Lett. 52, 2022 (1984).

49. Tatischoff et al., to be published.

50. For instance, see A. Th. M. Aerts et al., Phys. Rev. D17, 260 (1978); Phys. Rev. Lett. 40, 1543 (1978); P. J. Mulders et al., Phys. Rev. D21, 2653 (1980); P. J. Mulders, Phys. Rev. D25, 1269 (1982); D26, 3039 (1982); I. L. Grach, Z. Phys. C21, 229 (1984).

51. For instance, see Ref. 14; S. Furuichi et al., Prog. Theor Phys. 67, 547 (1982); T. Otofuji et al., Prog. Theor. Phys. 70, 322 (1983); 73, (1985); J. A. Tjon and E. van Faessen, Phys. Lett. 120B, 39 (1983).

52. For instance, see T.-S. H. Lee, Phys. Rev. Lett. 50, 1571 (1983); Phys. Rev. C29, 195 (1984); and references therein.

53. J. M. Laget, Nucl. Phys. A296, 388 (1978).

FIGURE CAPTIONS

Figure 1 pp total cross sections for pure longitudinal initial spin states.

Figure 2 Energy dependence of $\Delta\sigma_L(pp)$ data taken at Argonne ZGS, LAMPF, SIN, and TRIUMF.

Figure 3 $\Delta\sigma_T(pp)$ data taken at Argonne ZGS and LAMPF

Figure 4 $\Delta\sigma_T(pp)$ data by the Rice group

Figure 5 (a) The measured spin-spin correlation parameter C_{LL}, together with the available phase-shift solutions before the data.

(b) The measured spin-spin correlation parameter C_{SL}.

(c) The measured spin-spin correlation parameter C_{SS} at 487, 639, and 791 MeV. Predicted curves using solid and dashed lines are by Arndt and Hoshizaki respectively.

Figure 6 $\Delta\sigma_L^{in}$ vs. incident proton momentum p_L. Closed circles: $\Delta\sigma_L^{in}$ (Ref. 9); open circles: $\Delta\sigma_L^{in} - \Delta\sigma_L$ $(pp \to \pi d)$ at 1.18 GeV/c; and squares: $\Delta\sigma_L^{in} - \Delta\sigma_L$ $(pp \to \pi d)$ (E. Aprile et al., preprint, Geneva Univ. (1984)). The solid (König and Kroll), dashed (Kloet and Silbar), and dash-dotted (Rinat et al.) lines are predictions of the integrated cross section $\Delta\sigma_L(pp \to NN\pi)$ from Ref. 10.

Figure 7 Argand diagrams of the $^1D_2$ and $^3F_3$ partial waves based on Hoshizaki's phase shifts (points are in lab momenta, GeV/c).

Figure 8 Argand diagrams of the $^1D_2$ (a) and $^3F_3$ (b) partial waves based on Arndt's phase shifts (points are in kinetic energy, MeV). The ellipses represent the errors in the real and imaginary

parts of the amplitudes for energy-independent solutions. The continuous curves represent the energy-dependent solutions.

Figure 9 Triplet structure at 2.0 GeV/c; the dotted curve is deduced from $\Delta\sigma_L$ data.

Figure 10 Energy dependence of $P(d\sigma/d\Omega)$ at $\vartheta_{c.m.} \approx 63°$.

Figure 11 Experimental values of $f_t = k^2(C_{NN} - C_{LL})\ d\sigma/d\Omega$ at 90° as a function of kinetic energy. The dotted curve is drawn to guide the eye. The dashed curve represents a fit by eye to the experimental values of $f_s = k^2(1 - C_{NN})d\sigma/d\Omega$ at 90°. (The statistical errors are comparable to those in f_t.)

Figure 12 $\alpha = k^2\ C_{LL}\ d\sigma/d\Omega$ at $\theta_{c.m.} = 90°$.

Figure 13 $\Delta\sigma_L$ (I = 0) together with $\Delta\sigma_L$ (I = 1).

Figure 14 Cross sections for $pp \to NN\pi$ vs. p_L. The solid lines represent the Deck model predictions and the dashed ones the Deck model with dibaryon admixture.

Figure 15 Cross section for $\gamma d \to pp\pi^-$ vs. $E\gamma$. The dotted curve is the prediction of the model (Ref. 53). The solid curves includes second-order scattering terms.

Figure 16 $\gamma d^\uparrow \to pn$ at $E\gamma = 550$ MeV $(\sqrt{s} = 2380$ MeV).

Figure 17 π^-d elastic scattering at backward angles.

Figure 18 Angular distribution of t_{20}(lab) at $T_\pi = 138$ and 120 MeV. Open circles, data of Ref. 33 at 142 MeV. The solid curve is a guide for the eyes.

Figure 19 The vector polarization for $\pi d \to \pi d$ (Smith et al., Ref. 33). The dotted curve represents the standard theoretical predictions (Faddeev amplitudes). The solid curve is obtained by the

admixture of $^1D_2$ and $^1G_4$ dibaryon resonances to the Faddeev amplitudes.

Figure 20 Polarization parameter in $pp \to d\pi^+$.

Figure 21 The excitation energy distribution for the "non-spectator" (p_s > 350 MeV/c) sample. The dashed and dotted lines represent the background originating from single and double scattering, respectively. The solid lines refer to the $dp \to pnp$ three-body phase space alone, and together with the two Breit-Wigner distributions.

Figure 22 The two-neutrons excitation energy distribution for the sample enriched in "non-spectator" events. The solid and dotted lines refer to the background calculated by using data from the $dp \to ppp\pi^-$ reaction and FOWL program, respectively.

Figure 23 The "$nn\pi^+$" invariant mass distribution for the events with P_s > 0.3 GeV/c and "$nn\pi$" system emitted backward in the dp cms. The solid and dotted lines have the same meaning.

Figure 24 Missing-mass spectra in double differential cross sections measured in the reaction ^3He (p,d)X (laboratory system). Data have been binned into 5-MeV intervals.

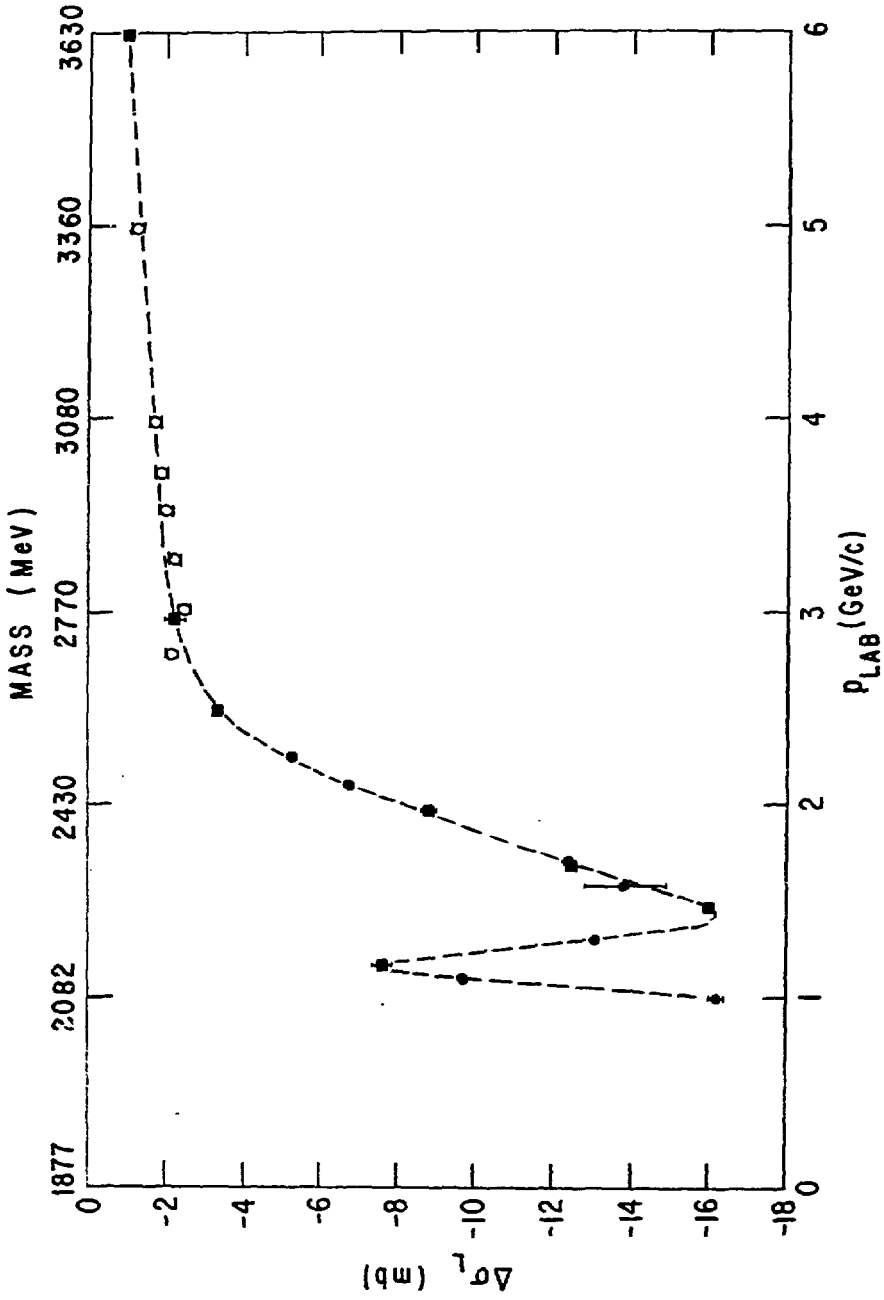
MASS (MeV)
1877
2082
2430
2770
3080
3360
3630
$\Delta\sigma_T$ (mb)
0
-2
-4
-6
-8
-10
-12
-14
-16
-18
p_{LAB} (GeV/c)
0
1
2
3
4
5
6

Figure 1

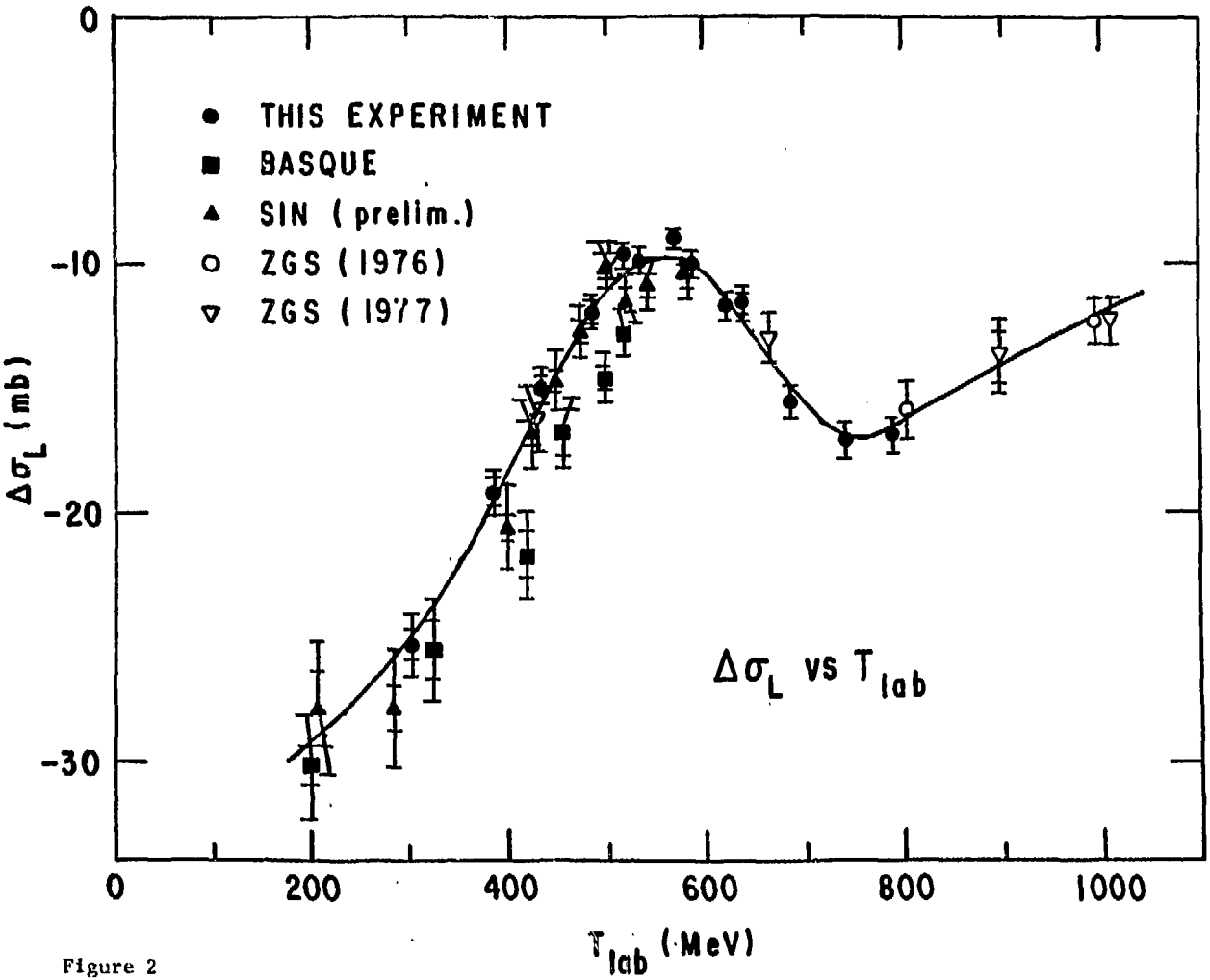
THIS EXPERIMENT
BASQUE
SIN (prelim.)
ZGS (1976)
ZGS (1977)
$\Delta\sigma_L$ vs T_{lab}
$\Delta\sigma_L$ (mb)
T_{lab} (MeV)
0
-10
-20
-30
0
200
400
600
800
1000

Figure 2

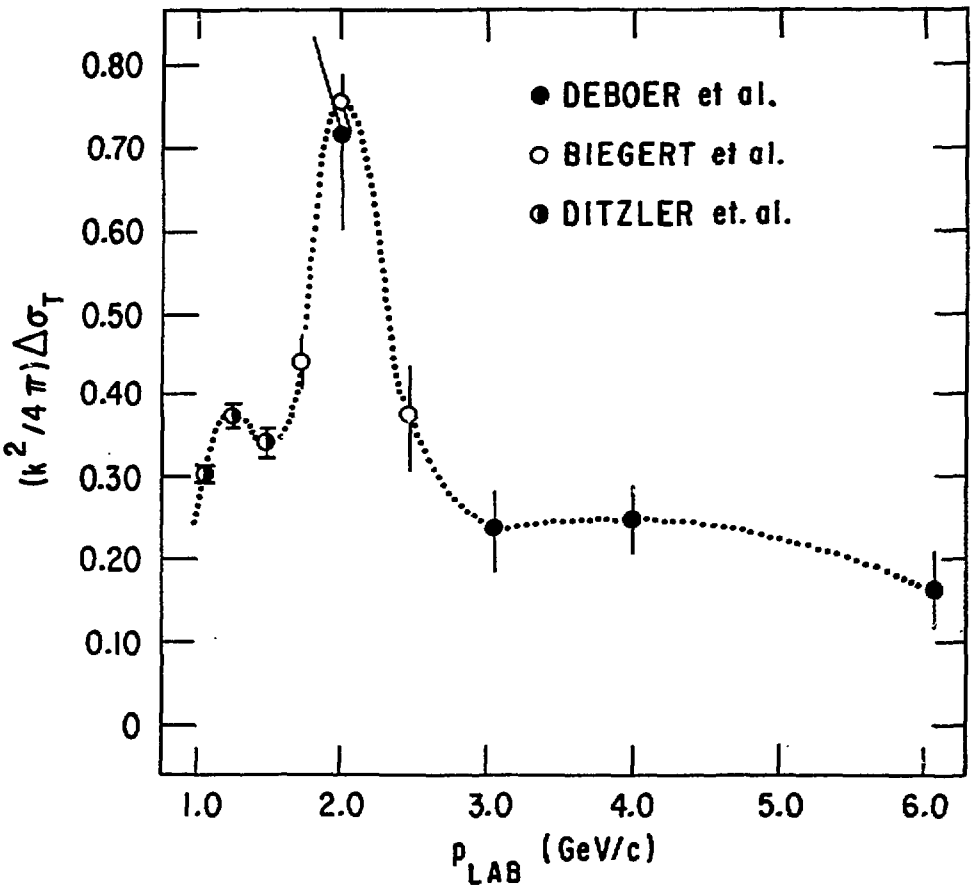
0.80
0.70
0.60
0.50
0.40
0.30
0.20
0.10
0
$(k^2/4\pi)\Delta\sigma_T$
● DEBOER et al.
○ BIEGERT et al.
◐ DITZLER et. al.
1.0
2.0
3.0
4.0
5.0
6.0
p_{LAB} (GeV/c)

Figure 3

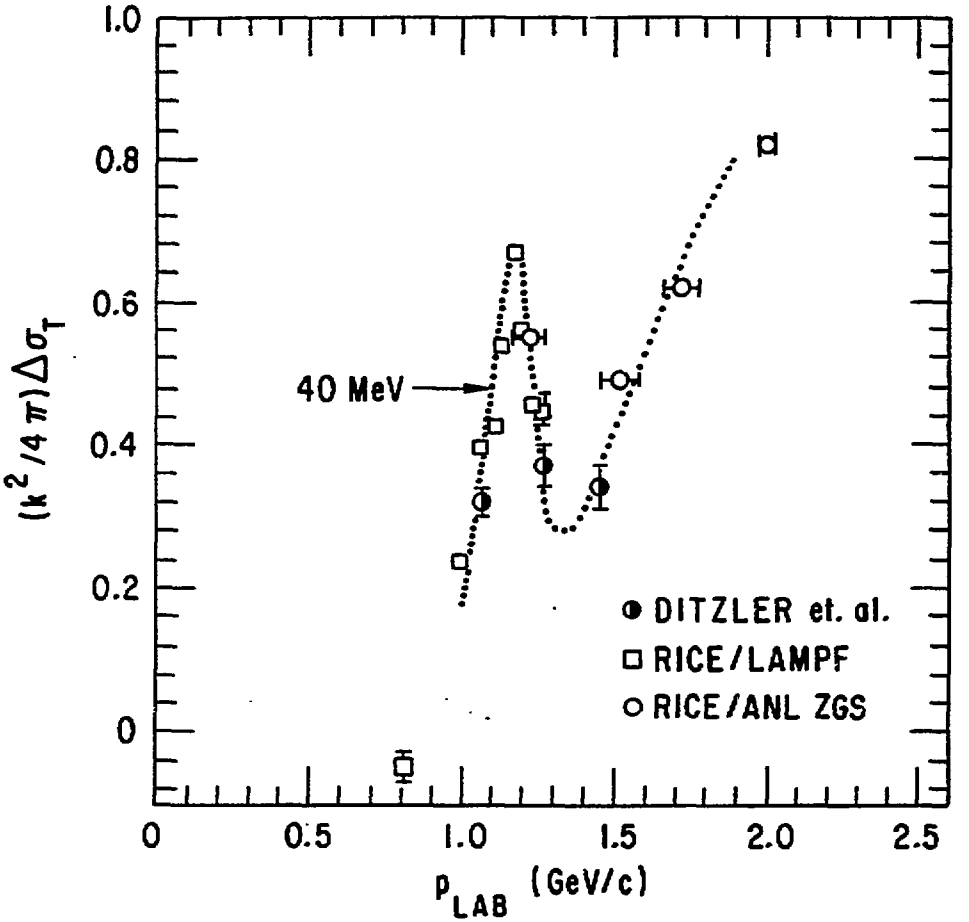
1.0
0.8
0.6
0.4
0.2
0
$(k^2/4\pi)\Delta\sigma_T$
40 MeV
DITZLER et. al.
RICE/LAMPF
RICE/ANL ZGS
0
0.5
1.0
1.5
2.0
2.5
p_{LAB} (GeV/c)

Figure 4

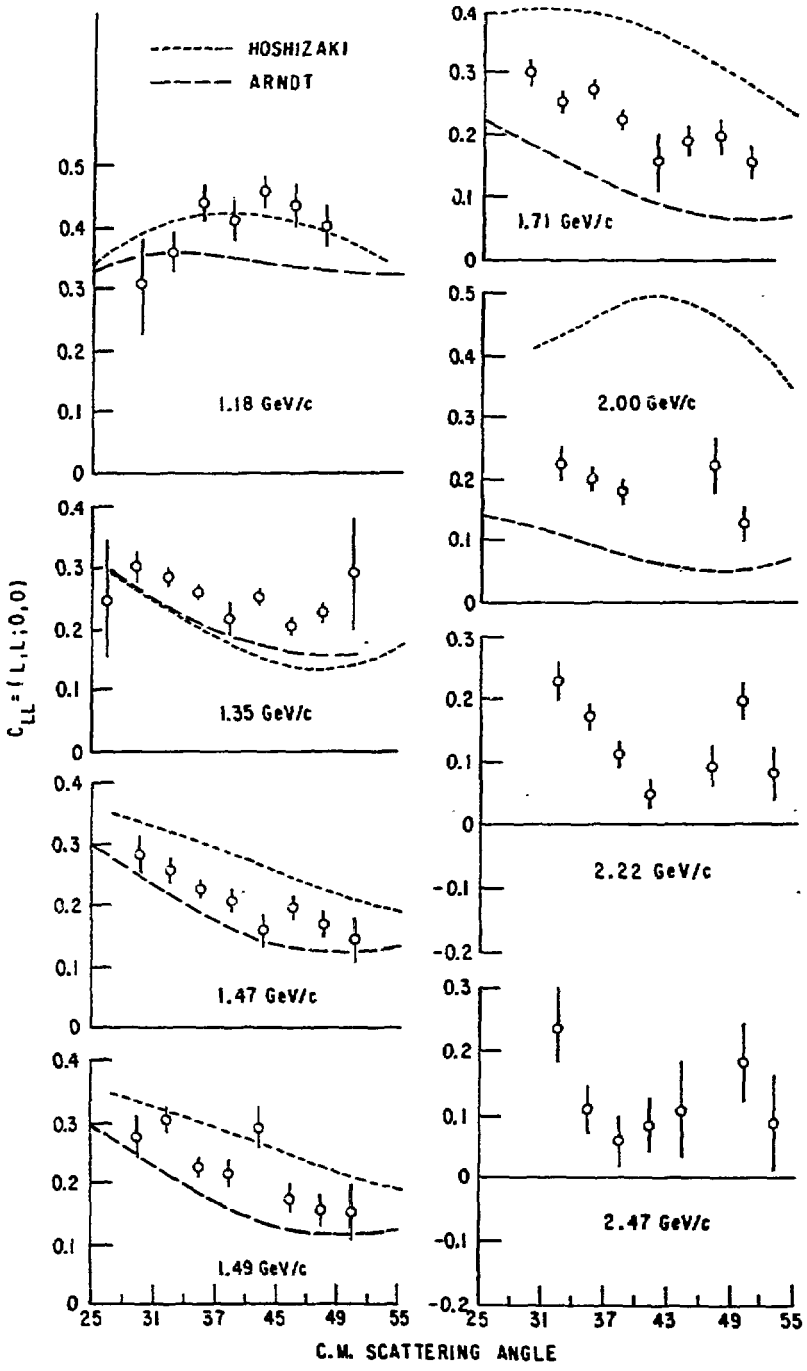
HOSHIZAKI
ARNDT
1.18 GeV/c
1.35 GeV/c
1.47 GeV/c
1.49 GeV/c
1.71 GeV/c
2.00 GeV/c
2.22 GeV/c
2.47 GeV/c
$C_{LL} = (L,L;0,0)$
C.M. SCATTERING ANGLE
25
31
37
43
45
49
55

Figure 5a

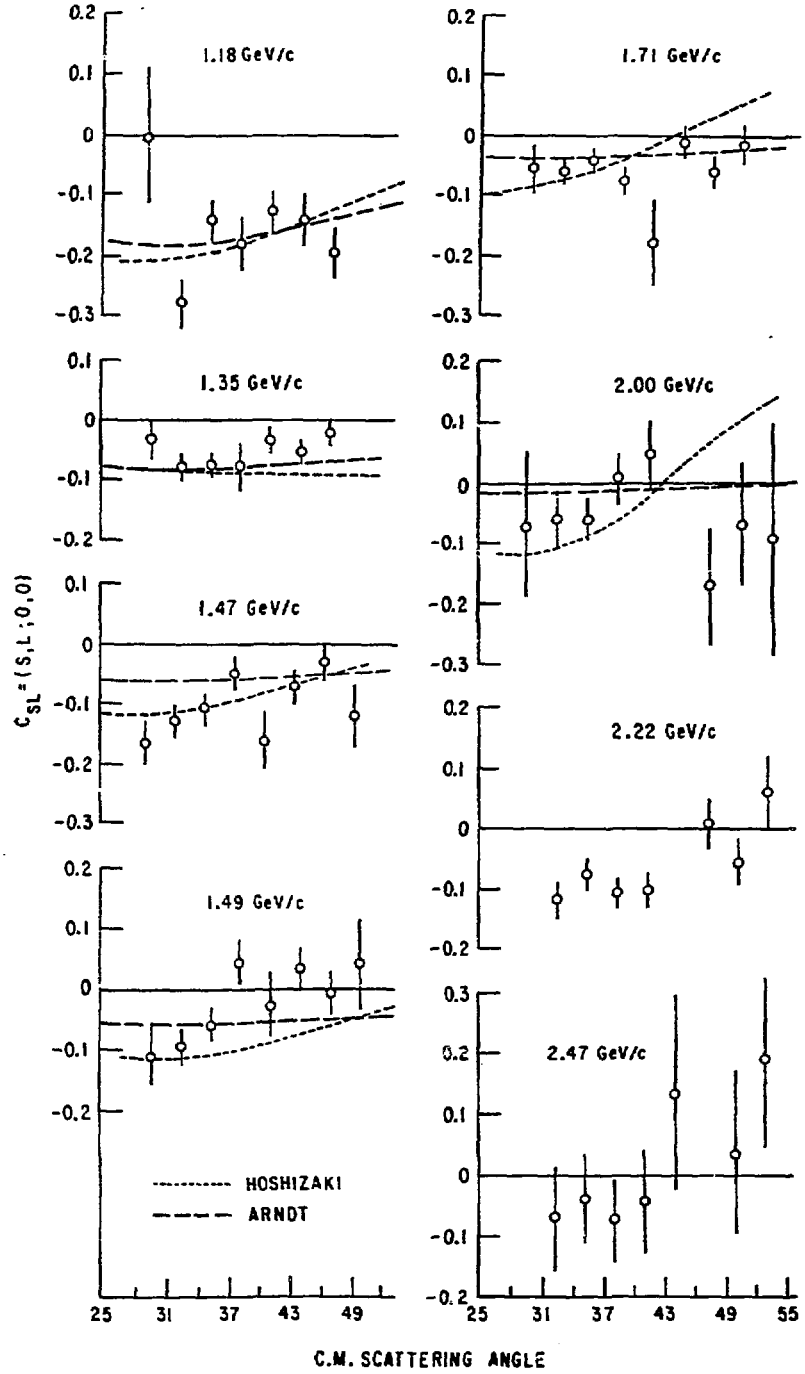
1.18 GeV/c
1.71 GeV/c
1.35 GeV/c
2.00 GeV/c
1.47 GeV/c
2.22 GeV/c
1.49 GeV/c
2.47 GeV/c
HOSHIZAKI
ARNDT
$C_{SL}=(S,L;0,0)$
C.M. SCATTERING ANGLE

Figure 5b

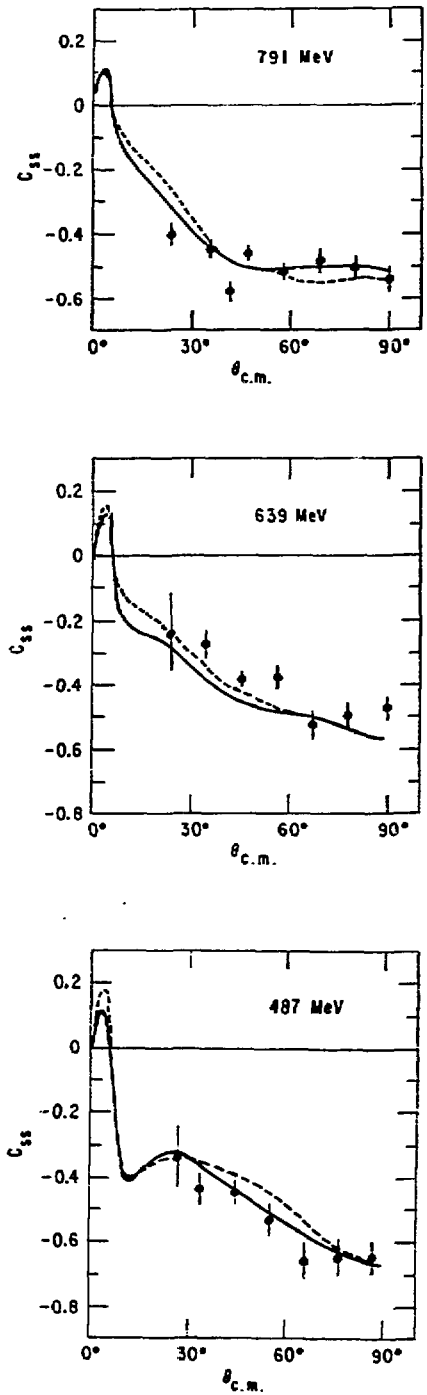

Figure 5c

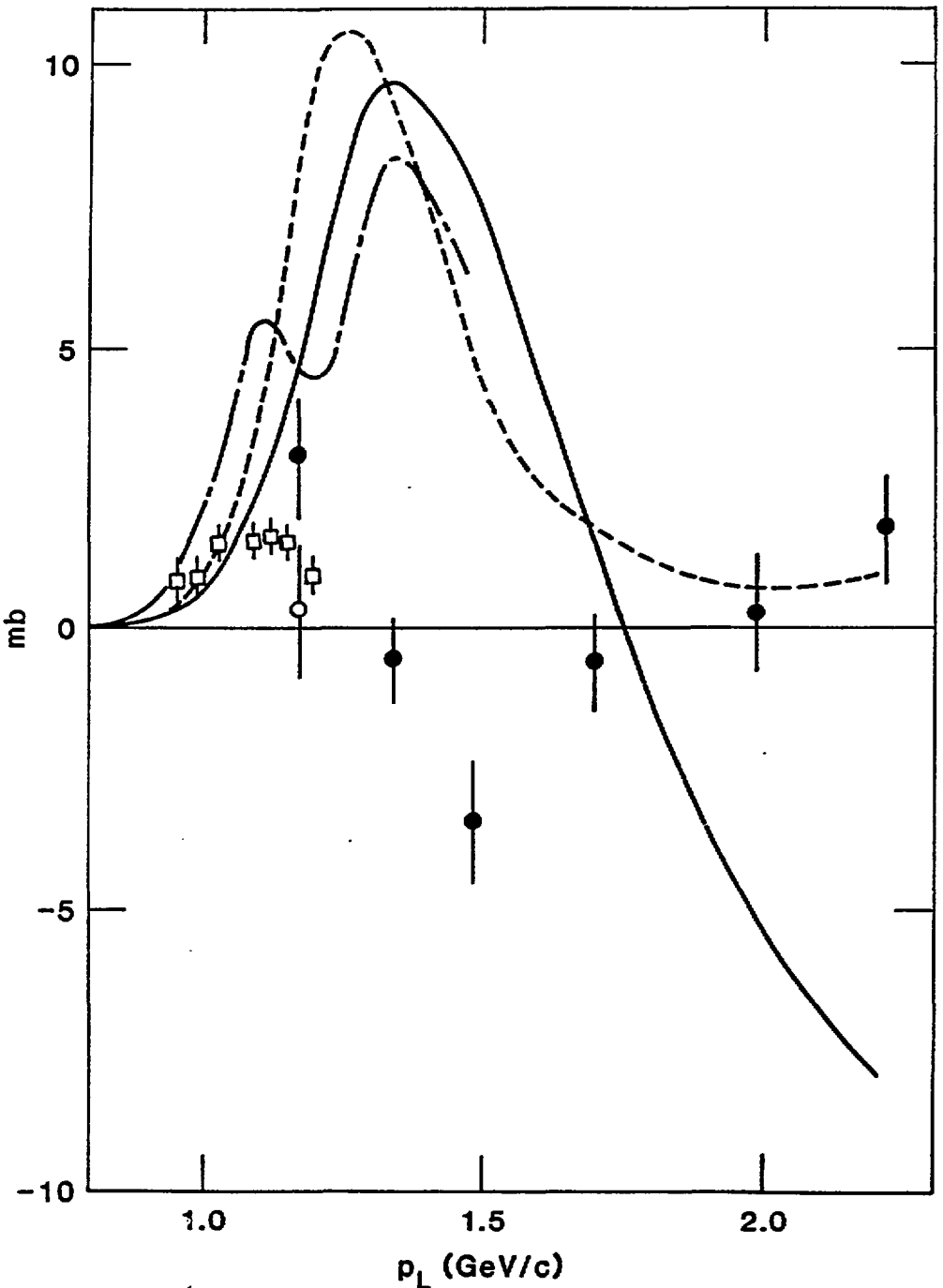

Figure 6

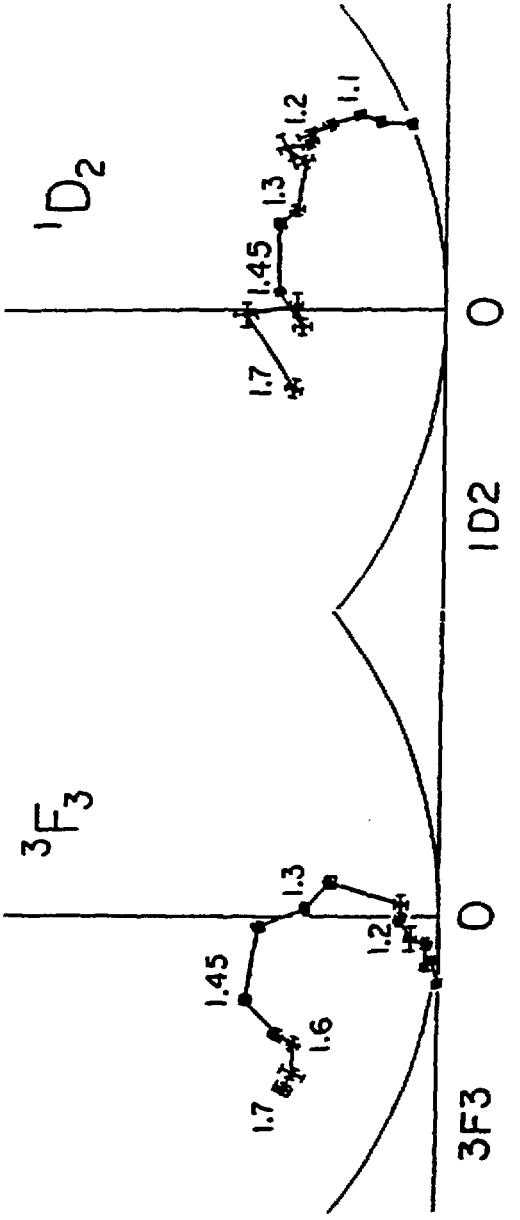

Figure 7

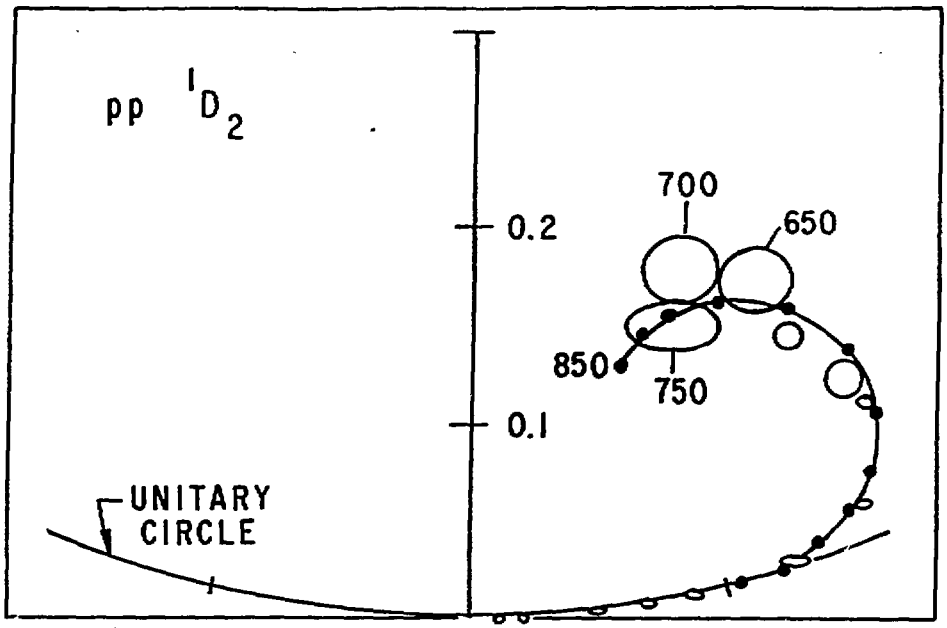
pp $^1D_2$
0.2
0.1
700
650
850
750
UNITARY
CIRCLE

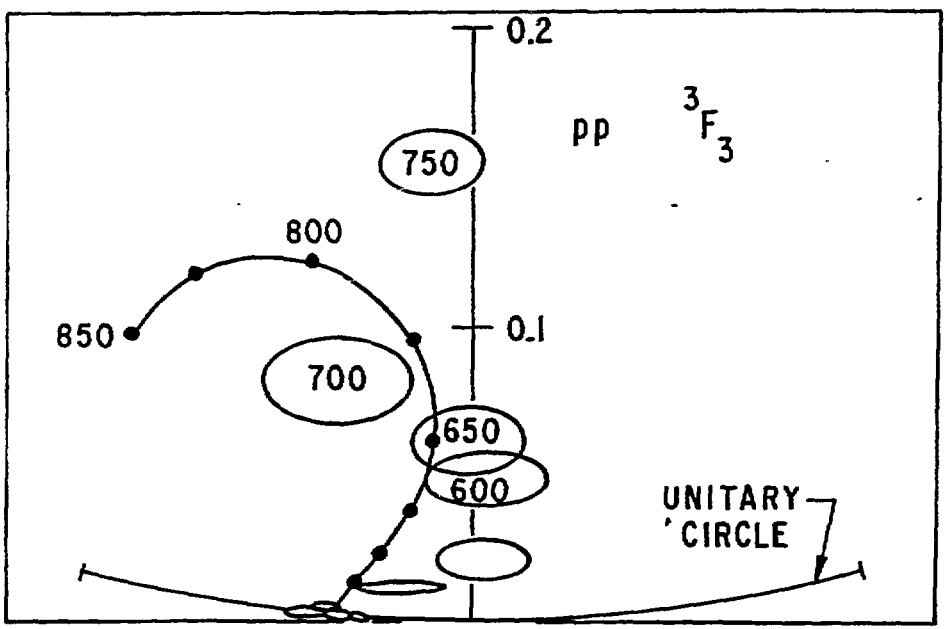
0.2
pp $^3F_3$
750
800
850
0.1
700
650
600
UNITARY
CIRCLE

Figures 5a/b

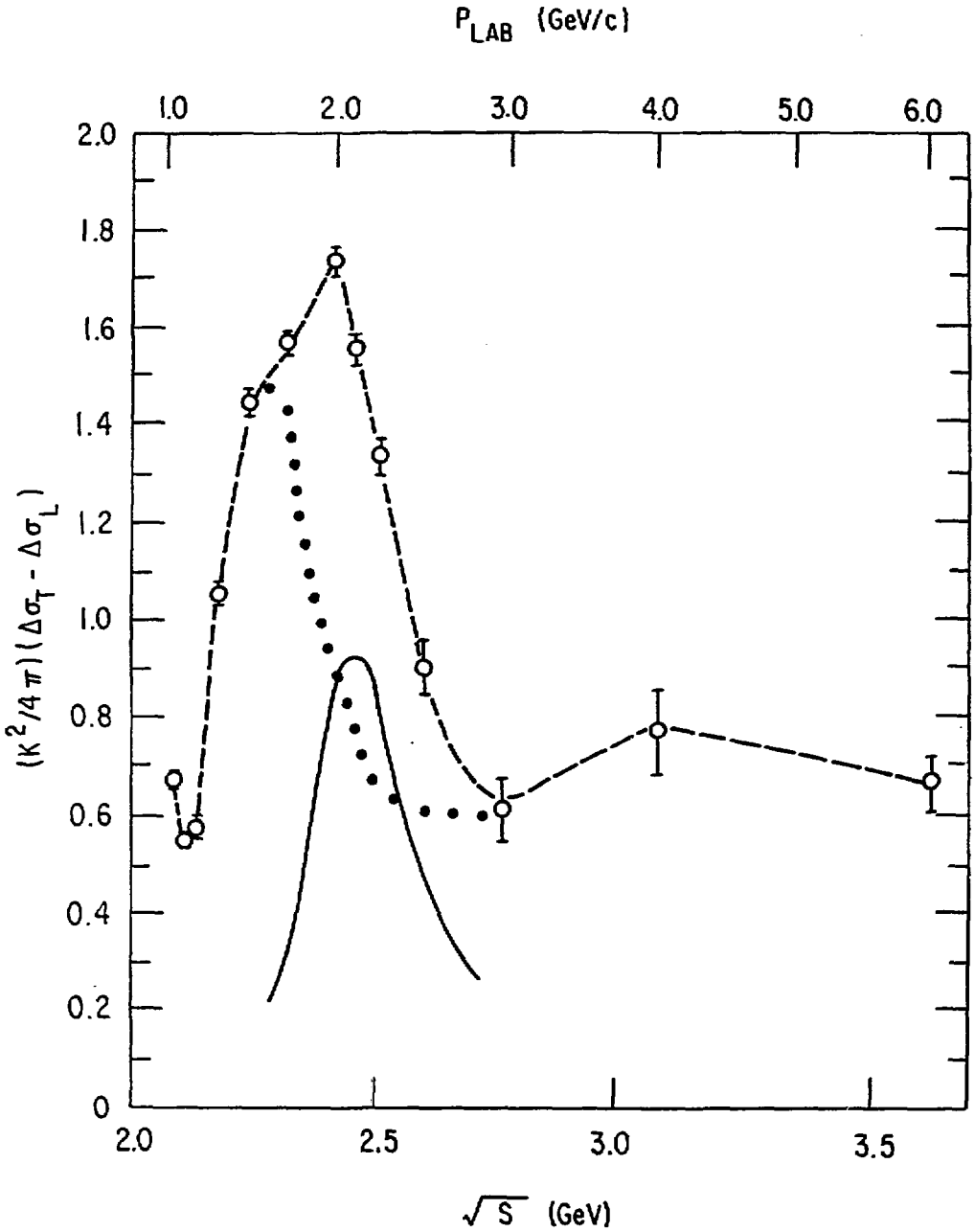
P_{LAB} (GeV/c)
1.0
2.0
3.0
4.0
5.0
6.0
2.0
1.8
1.6
1.4
1.2
1.0
0.8
0.6
0.4
0.2
0
$(K^2/4\pi)(\Delta\sigma_T - \Delta\sigma_L)$
2.0
2.5
3.0
3.5
$\sqrt{S}$ (GeV)

Figure 9

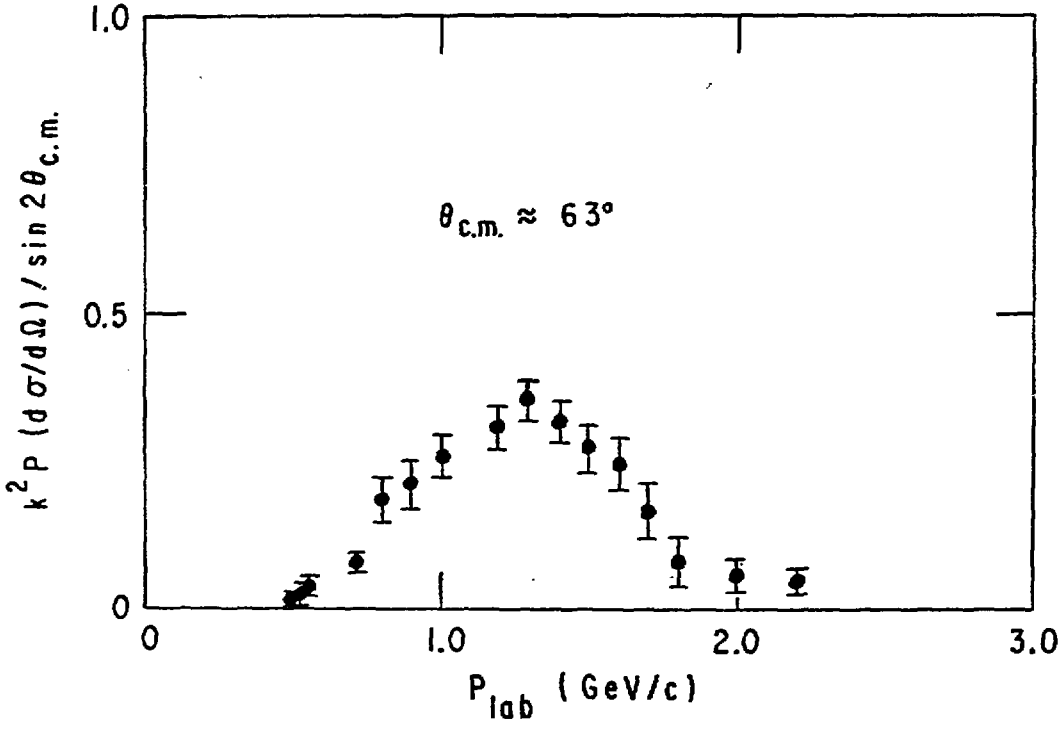
1.0
0.5
0
0
1.0
2.0
3.0
$k^2 P\ (d\sigma/d\Omega) / \sin 2\theta_{c.m.}$
$\theta_{c.m.} \approx 63°$
P_{lab} (GeV/c)

Figure 10

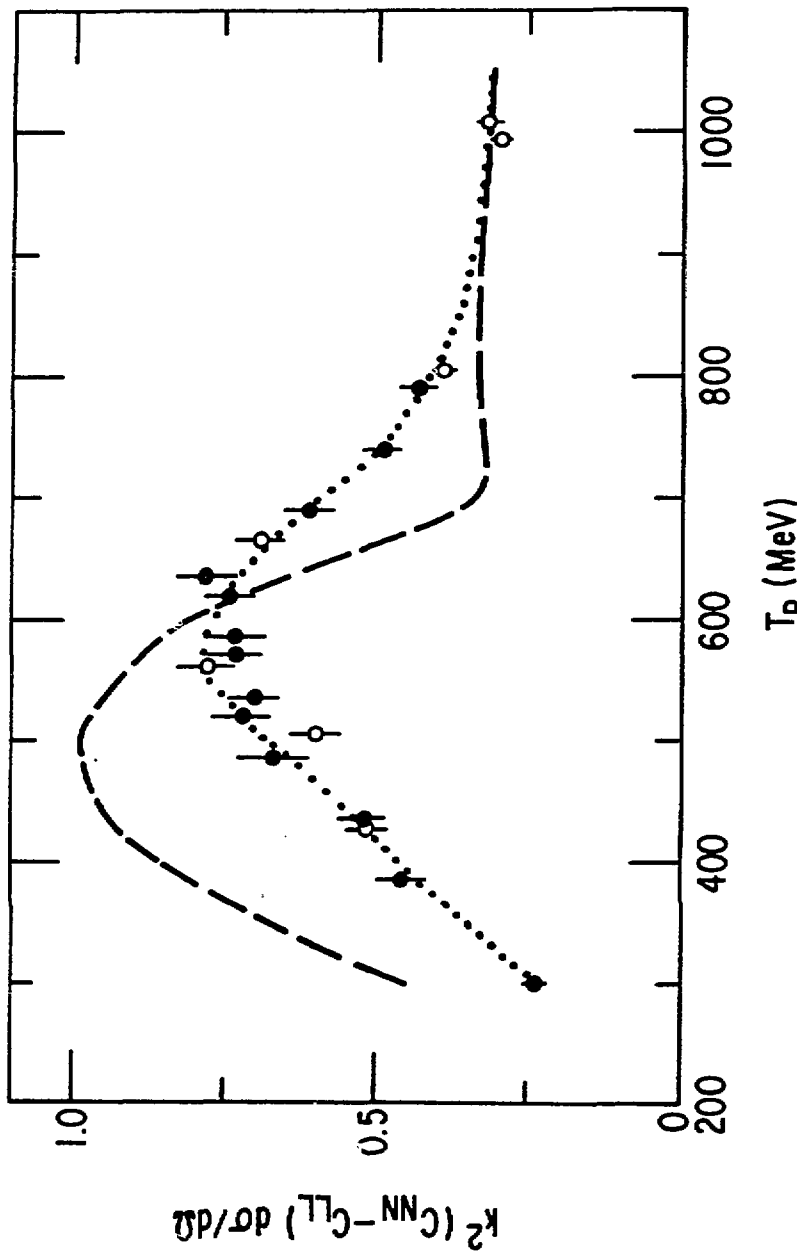

Figure 11

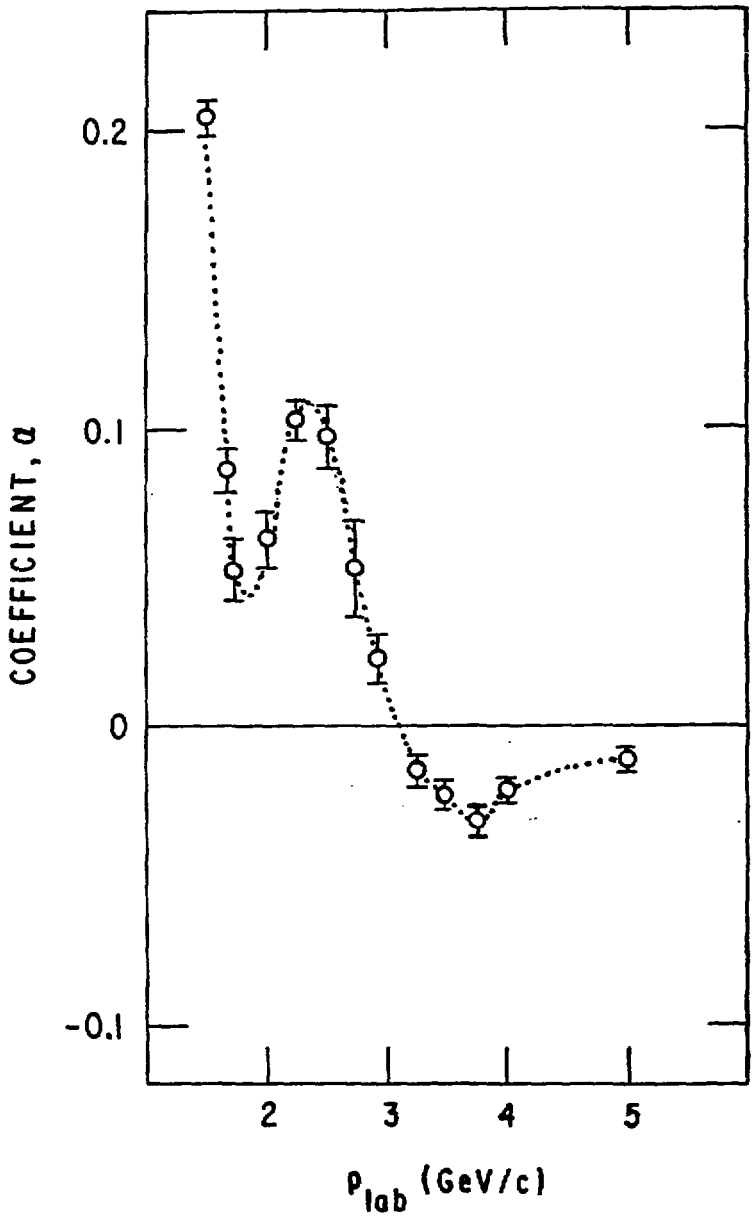

Figure 12

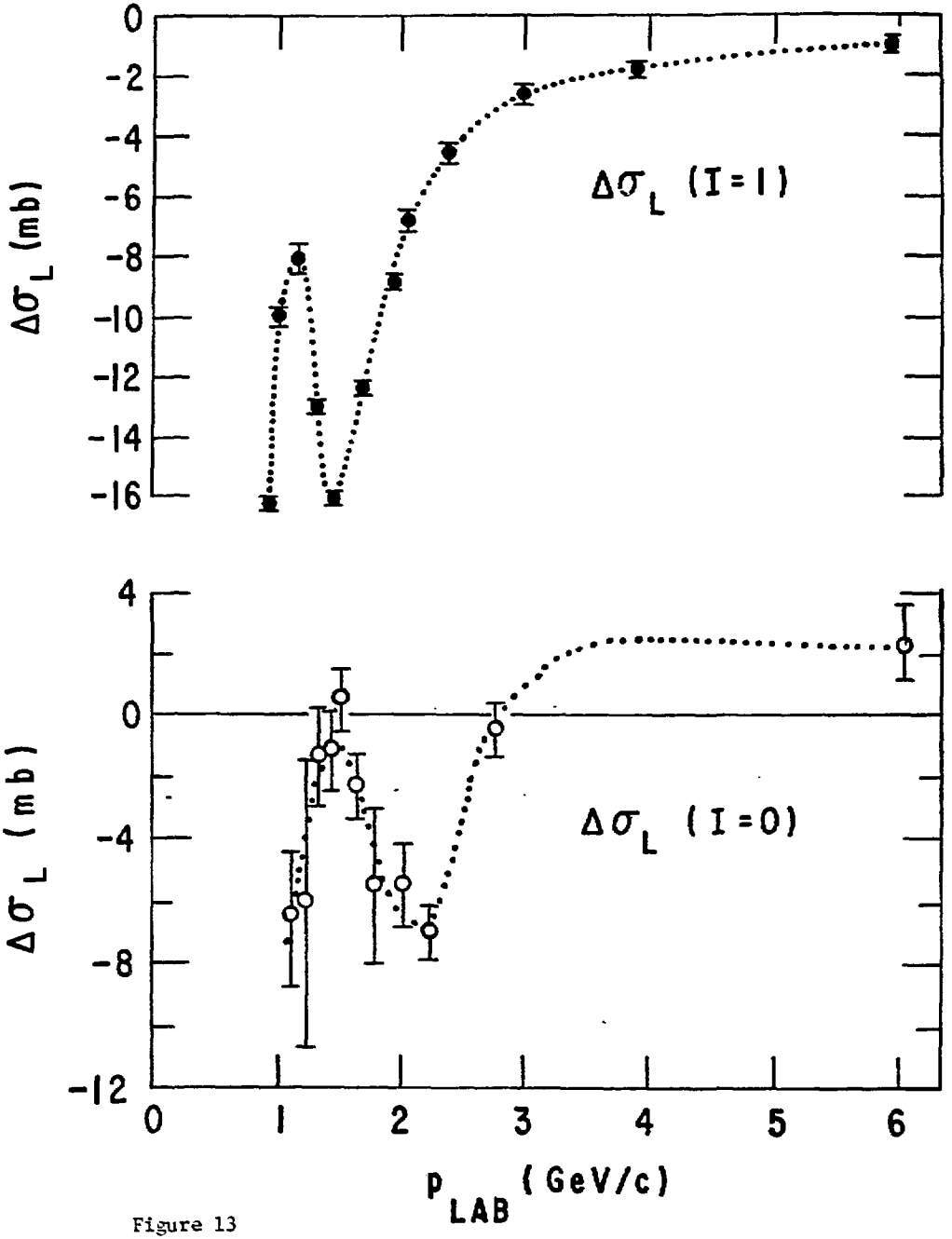
0
-2
-4
-6
-8
-10
-12
-14
-16
$\Delta\sigma_L$ (mb)
$\Delta\sigma_L$ (I=1)
4
0
-4
-8
-12
$\Delta\sigma_L$ (mb)
$\Delta\sigma_L$ (I=0)
0
1
2
3
4
5
6
p_{LAB} (GeV/c)

Figure 13

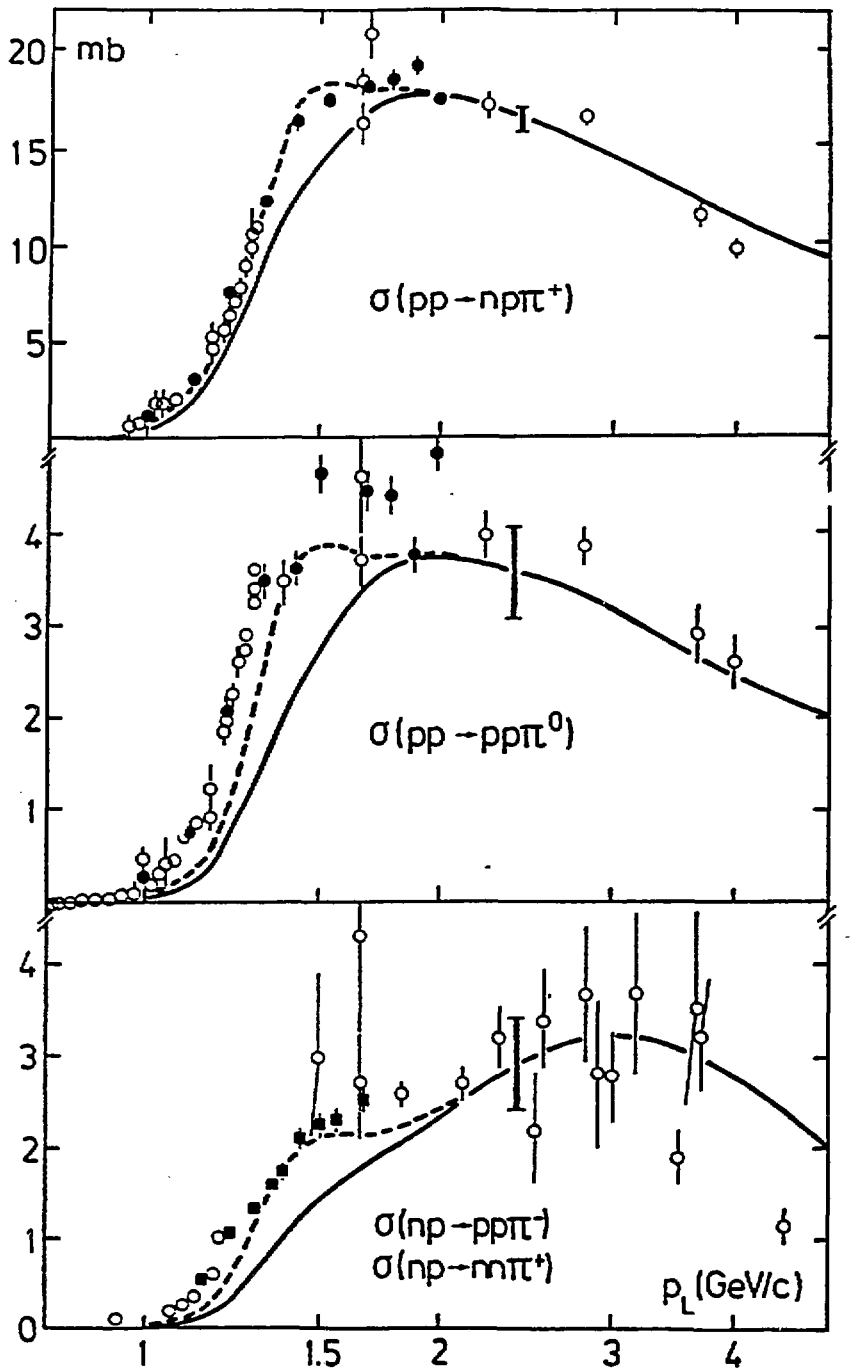
mb
20
15
10
5
σ(pp→npπ⁺)
4
3
2
1
σ(pp→ppπ⁰)
4
3
2
1
0
σ(np→ppπ⁻)
σ(np→nnπ⁺)
1
1.5
2
3
4
p_L (GeV/c)

Figure 14

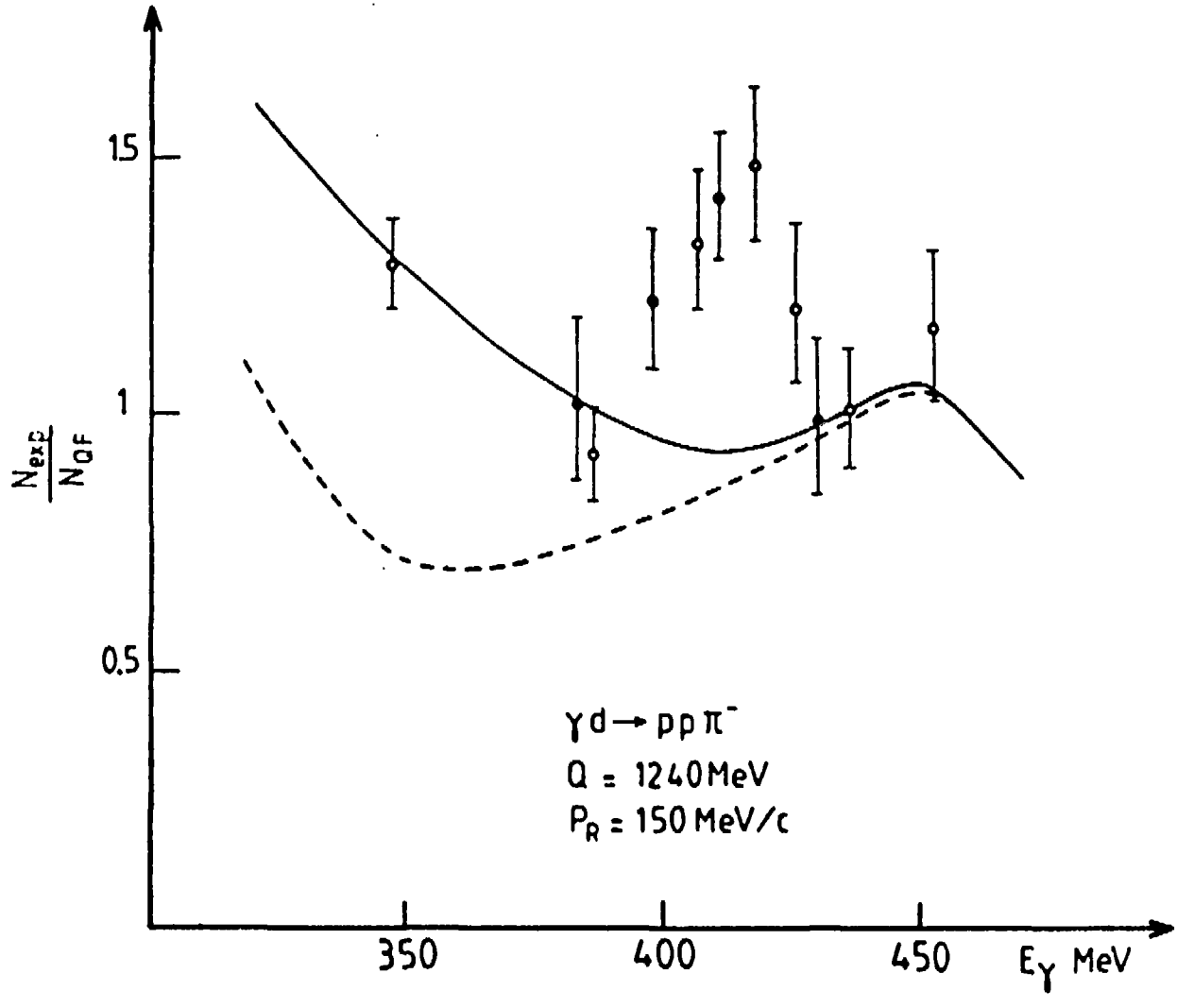
1.5
1
0.5
$\frac{N_{exp}}{N_{QF}}$
$\gamma d \rightarrow pp\pi^-$
Q = 1240 MeV
P_R = 150 MeV/c
350
400
450
E_γ MeV

Figure 15

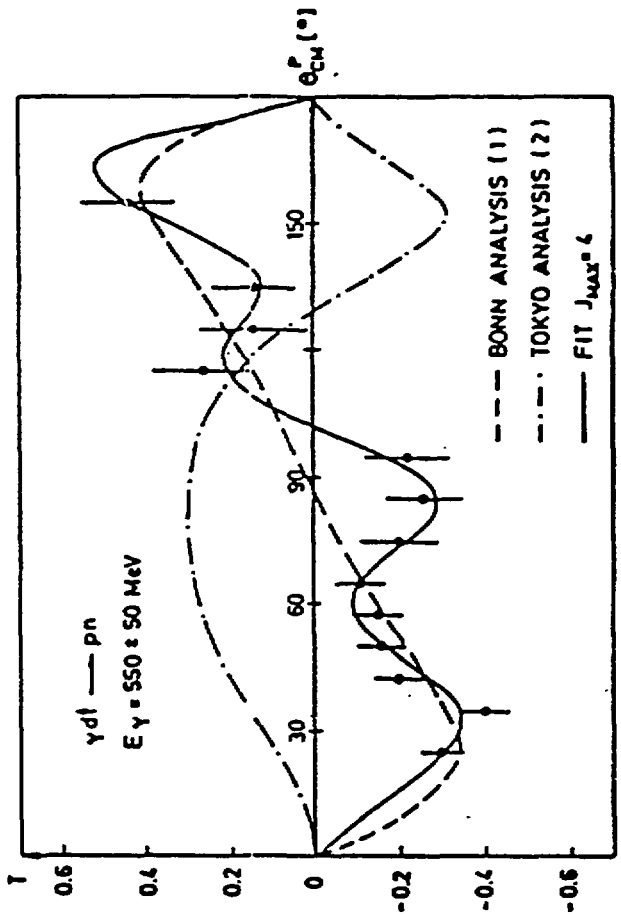
T
0.6
0.4
0.2
0
-0.2
-0.4
-0.6
30
60
90
150
θ^{p}_{CM} (°)
γd↑ —— pn
E_γ = 550 ± 50 MeV
--- BONN ANALYSIS (1)
-·-·- TOKYO ANALYSIS (2)
—— FIT J_{max} 4

Figure 16

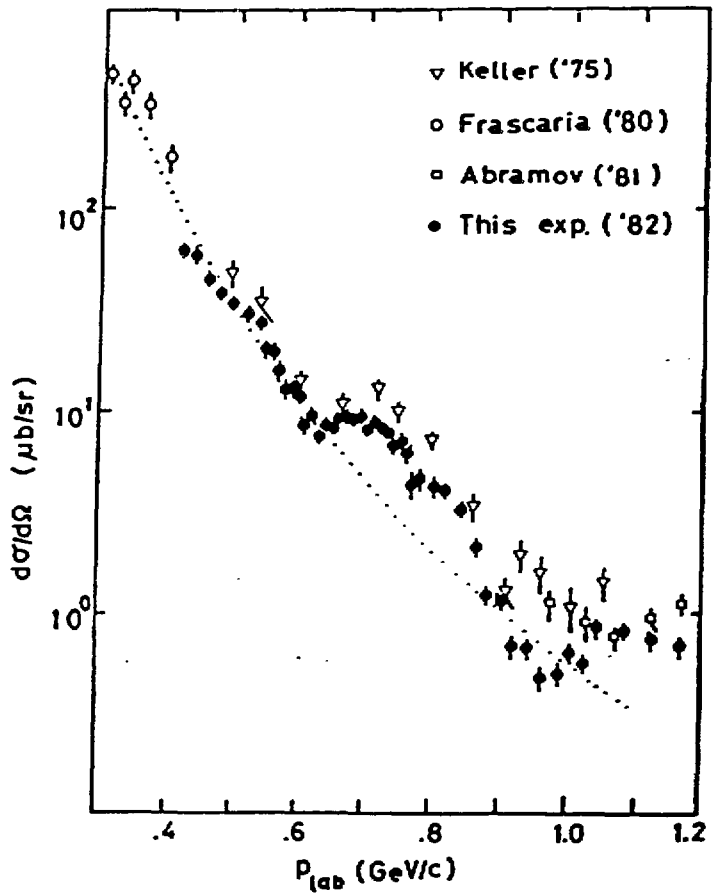
Keller ('75)
Frascaria ('80)
Abramov ('81)
This exp. ('82)
10^2
10^1
10^0
dσ/dΩ (μb/sr)
.4
.6
.8
1.0
1.2
P_{lab} (GeV/c)

Figure 17

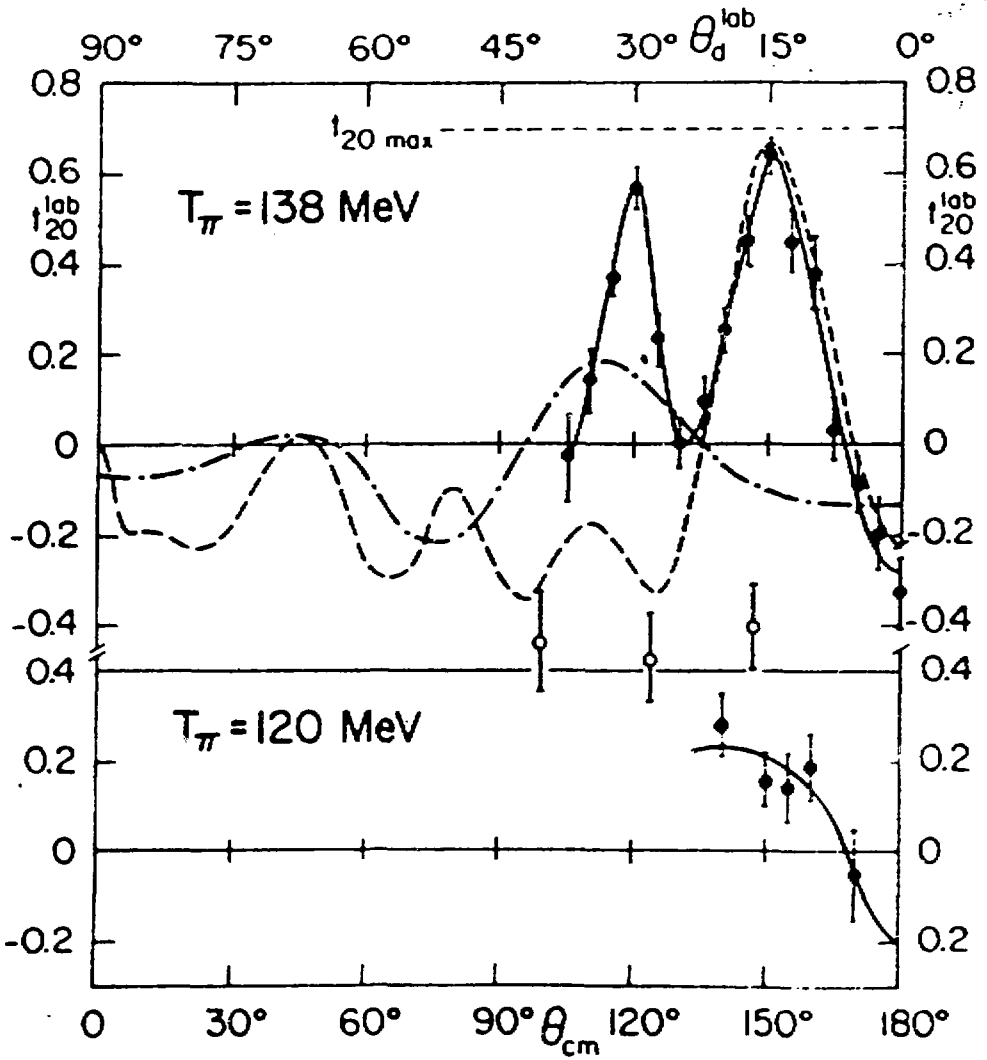
90°
75°
60°
45°
30°
θ_d^{lab}
15°
0°
0.8
0.6
0.4
0.2
0
-0.2
-0.4
$t_{20\ max}$
T_π = 138 MeV
t_{20}^{lab}
T_π = 120 MeV
0
30°
60°
90°
θ_{cm}
120°
150°
180°

Figure 18

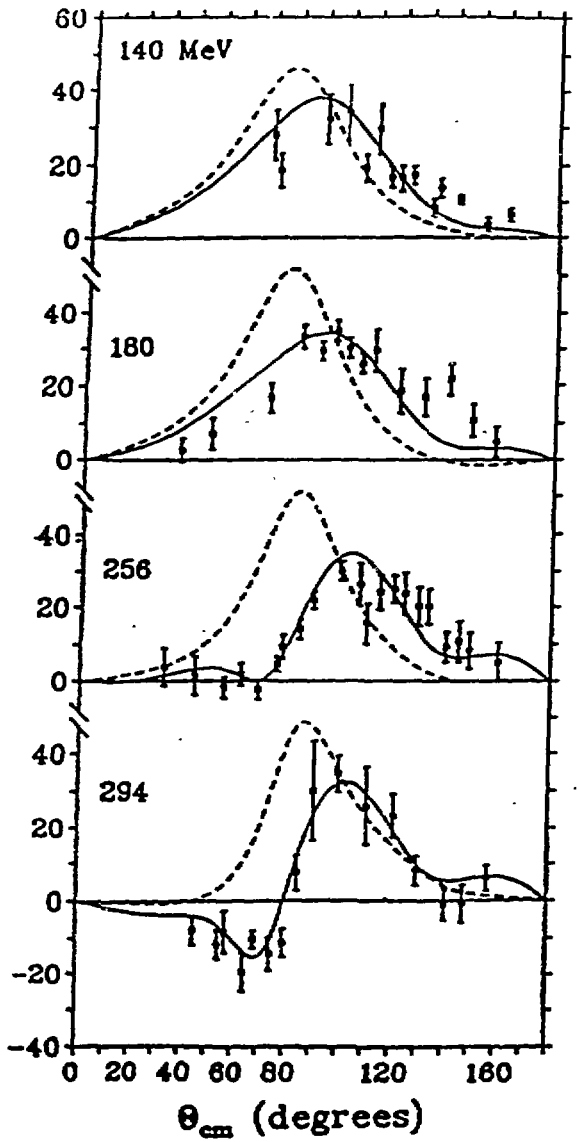
140 MeV
180
256
294
60
40
20
0
-20
-40
0 20 40 60 80 120 160
θcm (degrees)

Figure 19

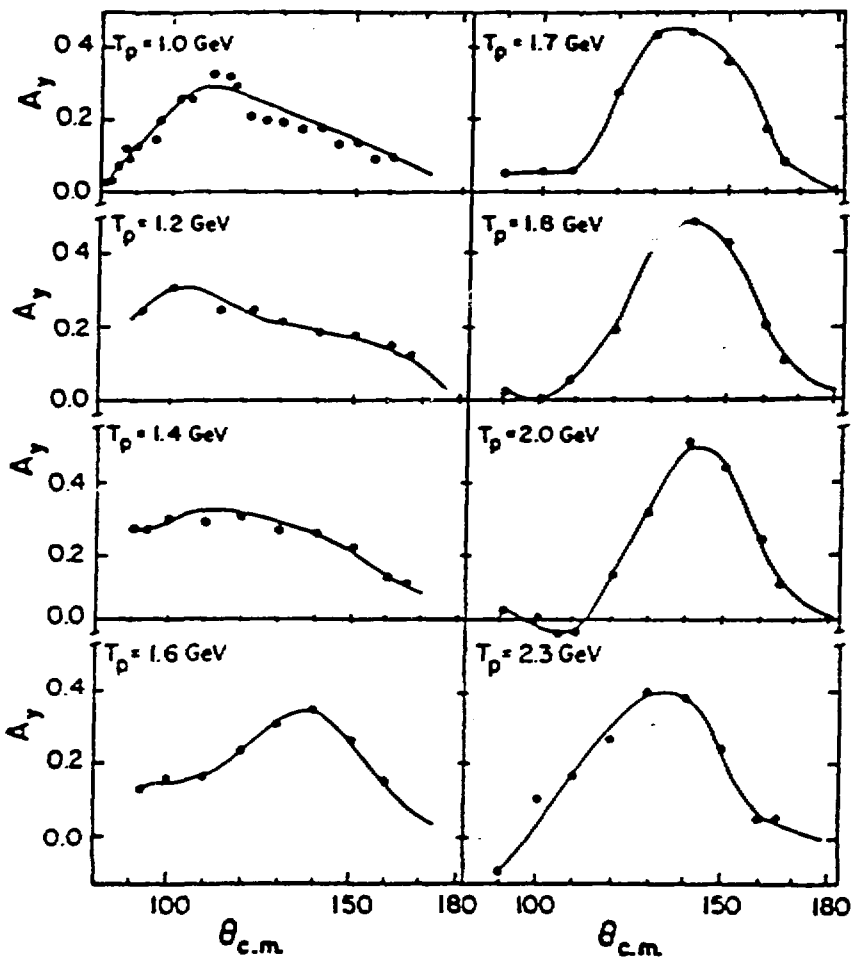
T_p = 1.0 GeV
T_p = 1.7 GeV
T_p = 1.2 GeV
T_p = 1.8 GeV
T_p = 1.4 GeV
T_p = 2.0 GeV
T_p = 1.6 GeV
T_p = 2.3 GeV
A_y
0.0
0.2
0.4
100
150
180
$\theta_{c.m.}$

Figure 20

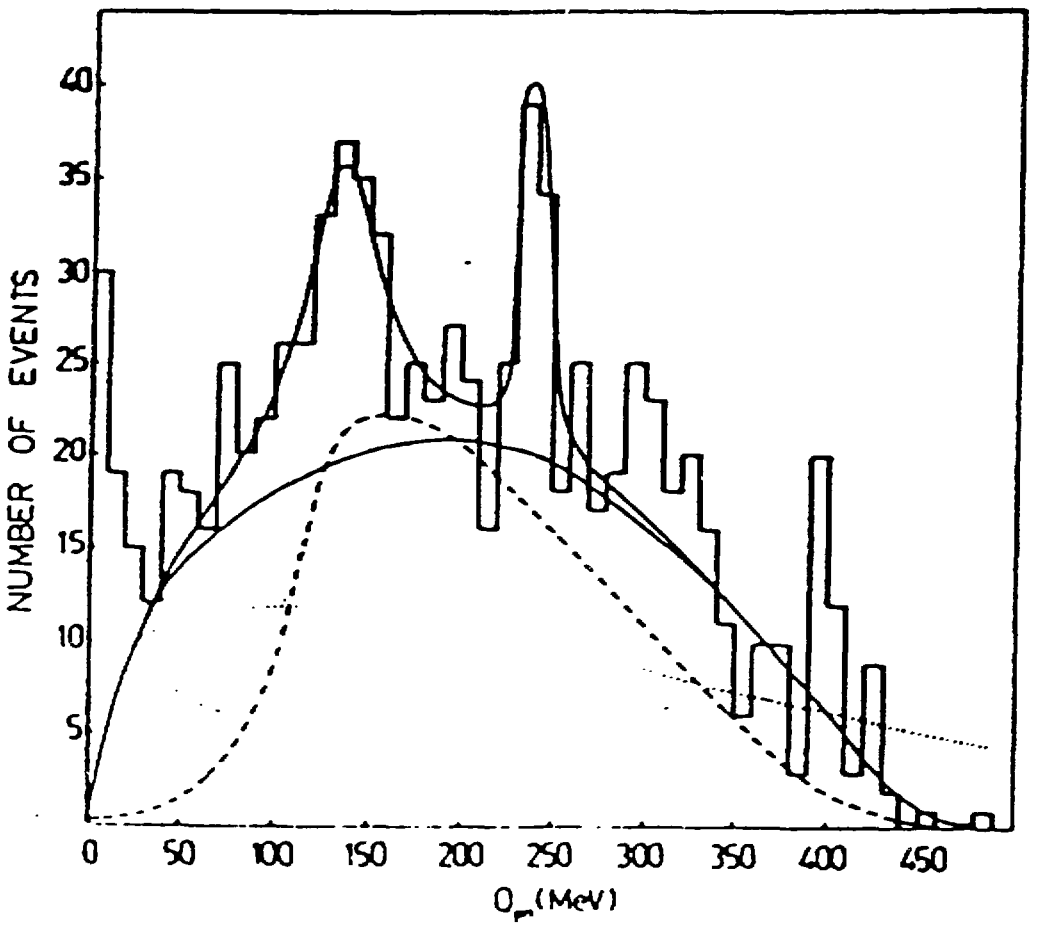
NUMBER OF EVENTS
40
35
30
25
20
15
10
5
0
50
100
150
200
250
300
350
400
450
Q_{pn} (MeV)

Figure 21

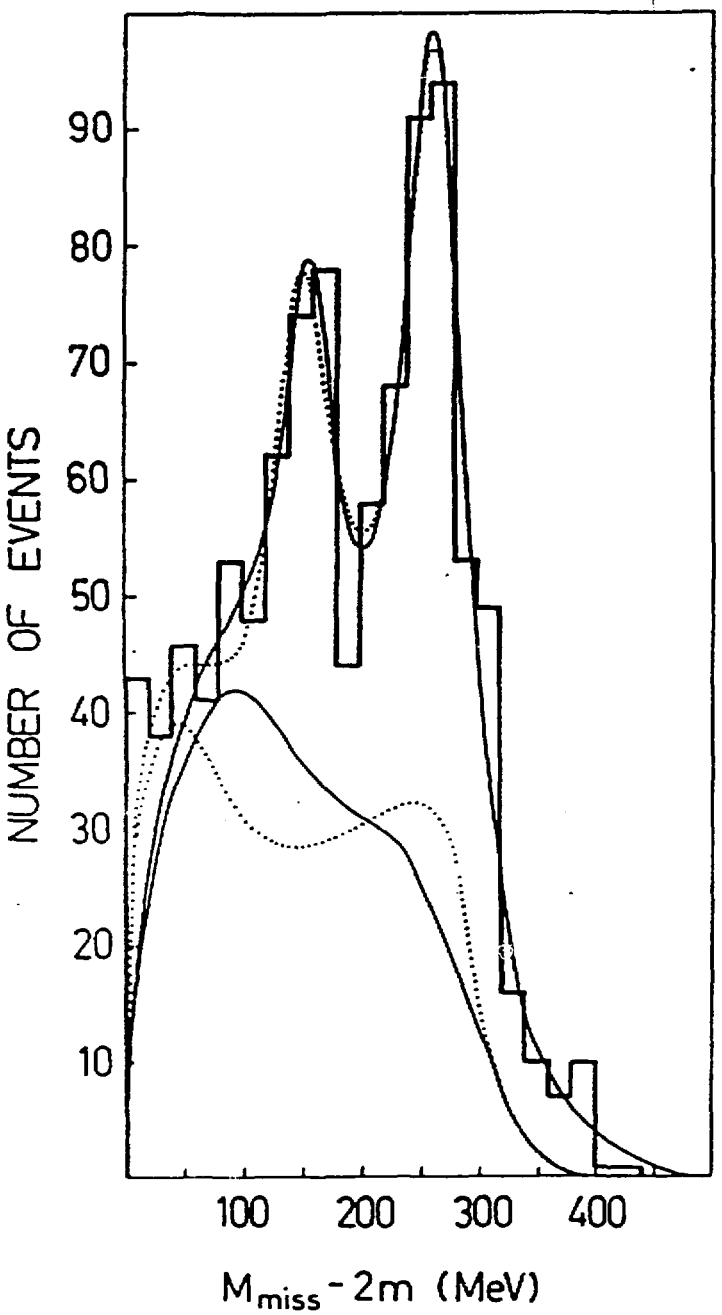
NUMBER OF EVENTS
90
80
70
60
50
40
30
20
10
100
200
300
400
$M_{miss} - 2m$ (MeV)

Figure 22

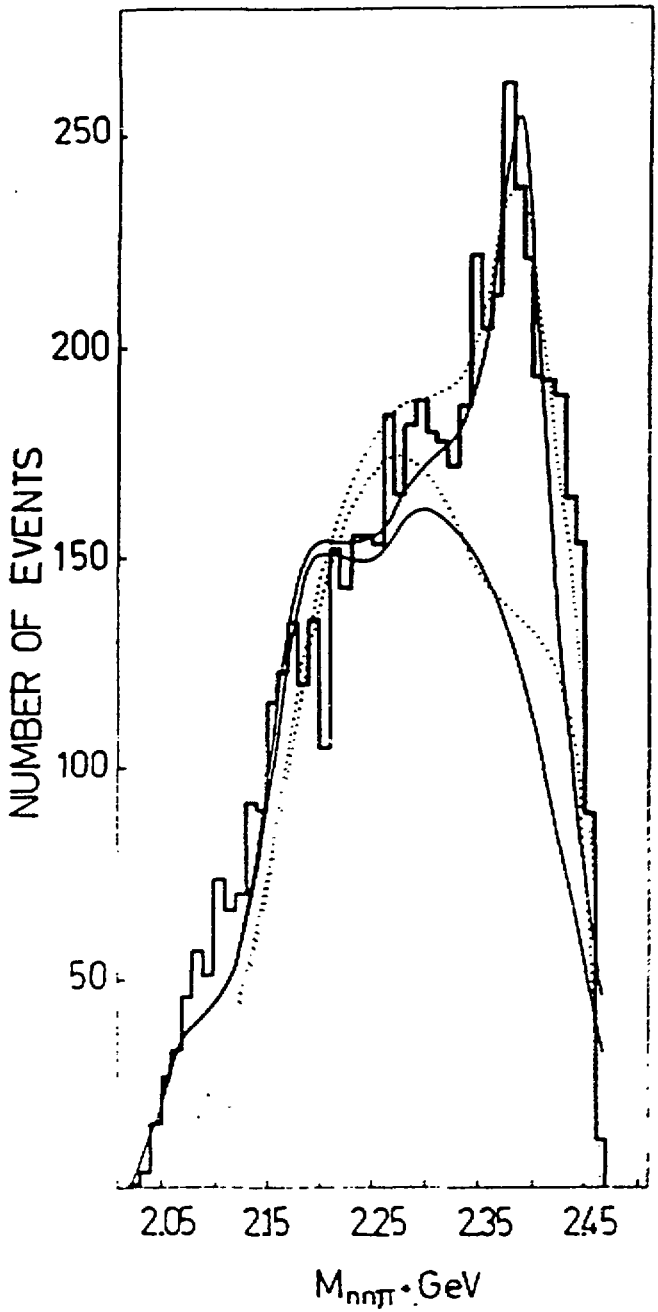
250
200
150
100
50
NUMBER OF EVENTS
2.05
2.15
2.25
2.35
2.45
$M_{nn\pi}$ · GeV

Figure 23

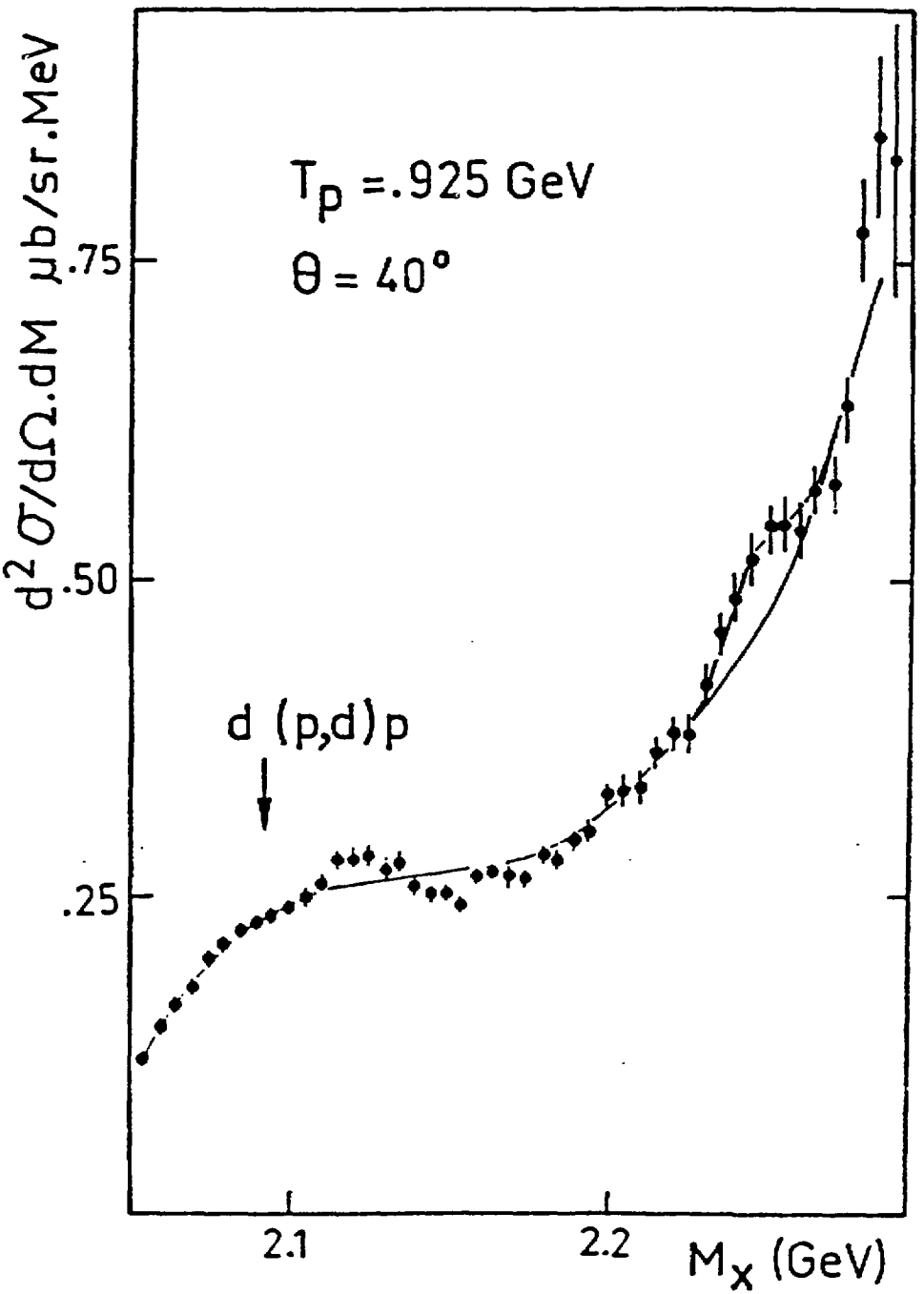
T_p =.925 GeV
θ = 40°
d (p,d) p
$d^2\sigma/d\Omega.dM$ μb/sr.MeV
.75
.50
.25
2.1
2.2
M_X (GeV)

Figure 24